MODELING ISOTROPIC ORGANS USING BEAM MODELS FOR THE HAPTIC SIMULATION OF BLUNT DISSECTIONS OF BILE DUCT

by

VISHAL DALMIYA

Presented to the Faculty of the Graduate School of

The University of Texas at Arlington in Partial Fulfillment

of the Requirements

for the Degree of

ELECTRICAL ENGINEERING

THE UNIVERSITY OF TEXAS AT ARLINGTON

August 2007

ACKNOWLEDGEMENTS

I have been highly motivated by my advisor Dr. Venkat Devarajan for this noble cause which deals with one of the most important aspects of surgery. He has always encouraged me to solve this problem which is highly interdisciplinary in nature. Being from the background of Electrical Engineering, it was hard to establish the mathematical model for simulating *blunt dissection*. In this regard, I am grateful to receive guidance from Dr. Kent Lawrence (Department of Mechanical and Aerospace Engineering, University of Texas at Arlington) and Dr. Guillermo Ramirez (Department of Civil Engineering, University of Texas at Arlington). All of my advisors have guided me and provided relevant information during the entire process of developing this concept. They have always been encouraging, helpful and patient in times of anxiety which has given me a good insight into the process of research.

From high school, I had the zeal to solve difficult problems. My physics teacher Professor Ajay Dhar is an exceptional man who helped me build the foundation of in depth understanding and analysis of any new topic at hand. He always wanted me to use my potential for the welfare of mankind. By doing this thesis I want to pay my tribute to this great man for the impact he made in my life and thought. I am also thankful to my family, which has been so supportive through out the process. Being the first engineer in the entire family is always a difficult proposition. But my parents have always given me the best of education and believed in me. Lastly, but not the least I want to thank my

fiancée Geeta, who I met at the University of Texas, Arlington. She has made a lot of difference to my confidence while solving this problem. There had been times of anxiety and worries and she always encouraged me and believed in my abilities to finish the work.

June 17, 2007

ABSTRACT

MODELING ISOTROPIC ORGANS USING BEAM MODELS FOR THE HAPTIC SIMULATION OF BLUNT DISSECTIONS OF BILE DUCT

Publication No. _____

Vishal Dalmiya, MS

The University of Texas at Arlington, 2007

Supervising Professor: Dr. Venkat Devarajan

Haptic modeling of organs using existing approaches is still not realistic and/or real time. We propose and develop the mathematical foundation of a new approach to modeling organs using beams. Beams are well known entities in Civil and Structural engineering. We develop their mathematical properties in the context of organ characteristics. The real time advantage arises from the fact that a single beam implementation eliminates hundreds, if not thousands of mass springs from the traditional mass spring models and, thousands of polygons from the finite element method (*FEM*). Even more importantly, our derivation works for both large and small deflections. This is important because we set out to simulate *blunt cutting* which

requires models for large deflections. Our new model, when simulated and compared with an *FEM* model provides comparable accuracy.

TABLE OF CONTENTS

LIST OF ILLUSTRATIONS

LIST OF TABLES

CHAPTER 1

INTRODUCTION

1.1 Background

Dissection is a process of separation of the tissues with homeostasis [23]. Homeostasis is defined as the process of keeping the internals of living beings within certain tolerable limits. Thus internal equilibrium of the body is maintained in homeostasis which ensures proper functioning of the overall system. *Blunt dissection* (Fig 1.1) of organs and tissues is a complex procedure in which we have to maintain a precise control over the instrument in terms of applied force and its placement. It needs good hand – eye coordination. The force required for dissecting a particular type of tissue or organ also needs the knowledge about its properties. Inadvertent application of a large force may cause excess bleeding and severe damage to connected tissues.

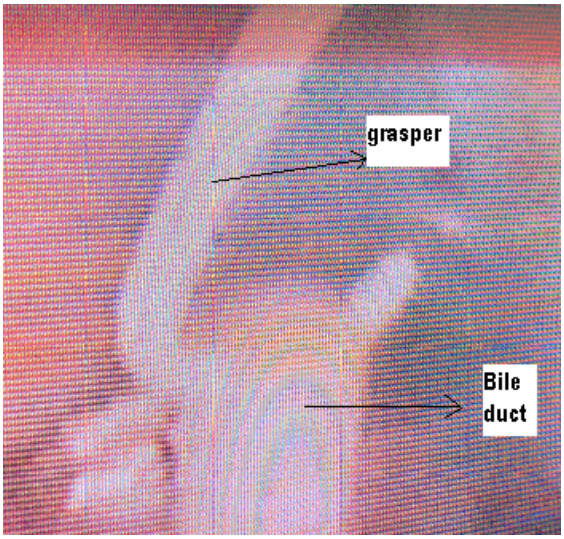

Fig 1.1 Video snapshot of *blunt dissection* of *bile duct*

Dissection and manipulation of tissue or organ within a confined space requires a two handed approach: one assisting and one dissecting. A passive assisting instrument (usually a grasper) provides counter traction and exposure for the active dissecting instrument. In our application, we usually deploy a hook like grasper (active dissecting instrument) to implement *blunt dissection* (see figure 1.1). The grasper is placed almost in the middle of the *bile duct* which needs to get dissected. Then, we gradually continue to apply force in incremental steps till it tears the *bile duct* into two pieces.

1.2 Problem and overview of solution

Our research group's extensive work with mass-spring models gives us a good perspective on their use and shortcomings. Although mass-spring models have been widely used for real time simulation [4] [5] [6] [7], this approach can give large error in some cases. To overcome these errors Wang et al [16] [18] proposed a parameter optimization scheme which however only works for small deflection. Our aim is to simulate *blunt dissection* both in small and large deflection zone and so this approach cannot be used in our case. The other popular method for haptic simulation is the Finite Element Method (*FEM*) [2]. This method is very accurate but as of now, not achievable in real time with high fidelity. It is the shortcomings of the above two approaches that have led us to search for a completely new approach. We then came upon the use of beam in Civil Engineering. It occurred to us that a beam may be suitable for organ modeling. We believe the reason this has not been proposed before is because of the classic problem of the lack of sufficient interaction among scientific disciplines. Civil and Structural engineers have for decades studied beams, plates, etc. We have tried to

use their fundamental approaches for the calculation of deflection to model *blunt dissection*. The associated mathematical modeling, although complicated, do offer some very attractive properties which we believe will be useful for modeling organs. Deflection in Civil engineering could map to deflection in soft tissues. We will later show that this model works in real time like the mass spring models and with good accuracy like *FEM,* thus combining the desirable properties of both methods while avoiding the shortcomings of both. Our research aims at simulating *blunt dissection* of *bile duct* real time with good fidelity. Our beam model fits perfectly into the purpose.

CHAPTER 2

MASS SPRING MODEL

2.1 Introduction

Mass spring model has been in use for a long time for simulating the force deflection response for many types of tissues and organs [4] [5] [6] [7]. This model is an accumulation of several masses connected to each other with the help of springs. The mass spring model works on the basic principles of Newton's second law of motion. In the following section, we give a brief overview of how the mass spring model is utilized for real time simulation.

2.2 Working principle

Fig 2.1 below describes a simple mass spring model. It consists of mass (m_i) at node i and connected to adjacent mass (node j) through spring $k_{i,j}$.

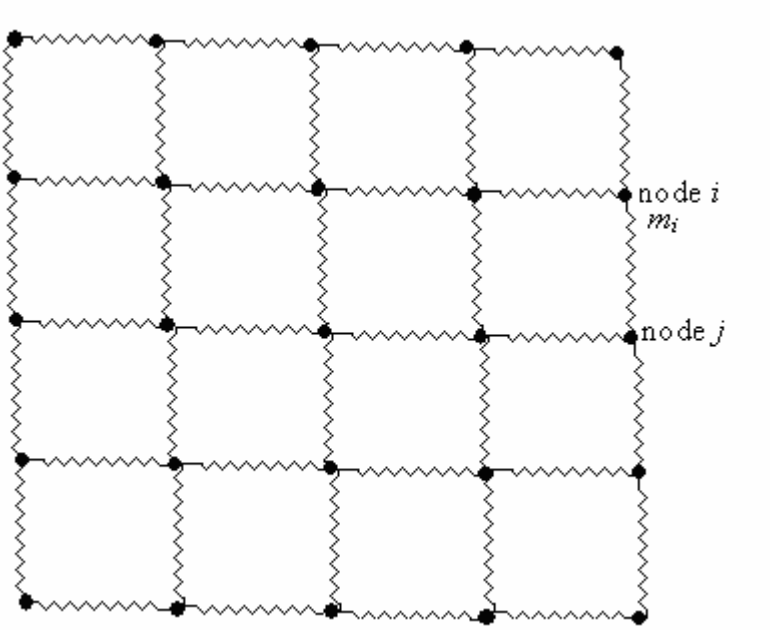

Fig 2.1 Mass spring model

Whenever a force is applied to any vertex (also called node), we use the general equation of dynamics to determine the deflection at that particular node and also the propagation effect of this force to other nodes present in the model. This governing equation can be written as:

$$m_i \frac{d^2x}{dt^2} + \lambda_i \frac{dx}{dt} = F_{total,i} \tag{2.1}$$

where m_i is the mass corresponding to that particular node, λ_i is the damping coefficient and $F_{total,i}$ is the total force acting at particular node *i*. $F_{total,i}$ consists of forces which are applied to the particular node externally ($F_{ext,i}$) and also the forces exerted on it due to the connected adjacent springs internally ($F_{\text{int},i}$). Hence, we can write $F_{total,i}$ as

$$F_{total,i} = F_{ext,i} + F_{\text{int},i} \tag{2.2}$$

Generally, the forces acting internally on the node are calculated using the knowledge of the position of that particular node along with its adjacent nodes. First, the displacement vector is calculated between two adjacent nodes. This displacement vector $\left(\vec{x}_j - \vec{x}_i\right)$ in turn is the stretched length of the spring connecting both the nodes (node *i* and *j* in this case). Knowing this displacement vector and the un-deformed length $l_{i,j}$ of the spring, the internal force can be calculated using the following equation:

$$F_{\text{int},i} = \sum_{j=1,..,n} k_{i,j}\left[\left|\vec{x}_j - \vec{x}_i\right| - l_{i,j}\right]\frac{\left(\vec{x}_j - \vec{x}_i\right)}{\left|\vec{x}_j - \vec{x}_i\right|} \tag{2.3}$$

Where $k_{i,j}$ is the spring constant between nodes *i* and *j* and $F_{\text{int},i}$ is the total internal force acting on the node *i* due to its adjacent nodes *j = 1, 2 …n*.

Once we know the total force acting on a particular node, we can then use several integration methods to calculate the position and velocity of that node at a particular instant. Few popular methods are discussed below:

2.2.1. Euler's method

Euler method of numerical integration for any node with mass *m* and total force F_{total} from step t_1 to t_2 can be mathematically written as:

$$x(t_1 + h) = x(t_1) + hv(t_1) \tag{2.4}$$

$$v(t_1 + h) = v(t_1) + h\frac{F_{total}(t_1) - \lambda v(t_1)}{m} \tag{2.5}$$

The above numerical integration is not very accurate and as a result may lead to instability.

2.2.2. Leap Frog method

This is an improvement to *Euler method* and the position and velocity can be mathematically expressed as

$$v(t_1 + \frac{h}{2}) = v(t_1 - \frac{h}{2}) + h\frac{F_{total}(t_1) - \lambda v(t_1)}{m} \tag{2.6}$$

$$x(t_1 + h) = x(t_1) + hv(t_1 + \frac{h}{2}) \tag{2.7}$$

This provides better accuracy and stability compared to *Euler method*.

2.2.3. Runge Kutta method

Runge Kutta method of numerical integration is also widely used for finding the positions and velocities of a particular node at different instants. There are two popular techniques for implicit integration, which are the second order and fourth order integration schemes. We are not going to discuss the details of the implementation of *Runge Kutta* method here. However, the main advantage of these advanced schemes is that the error in computation decreases helping in increasing stability of the system while allowing larger steps for simulation.

Besides the above mentioned popular techniques for numerical integration, there are other schemes like *Verlet*, *Richardson*, etc. Accuracy and stability of the mass spring model are important. However, one must ensure that the process is real time. So there is always a trade off between accuracy and computation time. A great deal of research has been done to reduce the computation time for simulation without incurring

instability [7] [12] but correct parameter optimization for the mass spring model to make it work in large deflection still remains a problem. This was one of our motivations for our research.

CHAPTER 3

FINITE ELEMENT METHOD

3.1 Introduction

Finite Element Method *(FEM)* [2] is a very popular technique of subdividing a continuous structure into substructures or elements. Each element in turn consists of nodes. There are two fundamental principles that are followed in the finite element analysis. First is the condition of *compatibility* and second is the condition of *equilibrium*. By compatibility, we mean that the nodes of two elements stay together where they are joined. And by equilibrium, we mean that any node of an element in the finite element analysis should be under equilibrium under the action of different external forces and moments. Following these two basic principles of compatibility and equilibrium and given different applied forces, moments and boundary conditions, we can compute the deflection and other entities acting on the particular node.

3.2 Assembly

In finite element analysis, we define the relation between externally applied forces on nodes and the deflection of the nodes using a stiffness matrix. So when we are assembling two or more elements, we need to identify the important nodes in the assembly. Once we achieve that, we draw the free body diagram of each node and look for the compatibility and equilibrium conditions of each node to find the stiffness

matrix. Knowing the stiffness matrix, for given values of external forces, moments or deflections, we can find the unknown reaction forces, deflections, etc.

3.3 Modeling technique

In the finite element method, given a structure we can create a model in a lot of different ways. We can use *beams, trusses, plates, shells, tetrahedral* and other elements to model any object. The modeling is very important because the accuracy of results obtained depends on the number of elements and interpolation points within an element. To increase accuracy, we can increase the number of elements in the mesh (called the *h – method*) or increase the number of interpolation points within a particular element (called *p – method*). Usually, if we use less number of elements or interpolation points within a mesh than the required number, there will be considerable error in the results obtained from such modeling techniques. The denser the meshing and interpolation points, the faster the results converge to the theoretical values. However the computation time becomes very high. In our application, accuracy is important but on the other hand computation burden is also of significant importance as we want the system to work real time. The computational time also depends on whether the solution is linear or non-linear. Non – linear solutions are used for large deflections and their convergence time is considerably high as compared to the computation of small deflection given the same number of elements and interpolation points forming the model. For all these reasons *FEM* is not suitable for our application because a real time, large and accurate deflection is not feasible using this approach. However, in some cases, when there is no topology change, i.e. cut and suturing operation, it is possible to

obtain real – time deformations by using pre-computation [10] because the stiffness matrix in the *FEM* scheme does not change.

CHAPTER 4

RAYLEIGH ENERGY METHOD

This chapter describes a method applied to the analysis of beams. Although this is well known in Civil and Structural Engineering, since this is one of the central concepts used in our own organ modeling, we provide this introduction to non – civil engineering readers.

4.1 Rayleigh's energy method applied to beams without axial loading

Rayleigh method [3] is very often used in analyzing static and dynamic behavior of beams under bending. In our application which is based on simulating *blunt dissection,* we deal with the static problem. At first we will cite the use of this method to determine the static behavior of the beam under simple bending. In *blunt dissection*, the beam is however also subjected to axial forces which we will cover later, in section 4.2 of the chapter.

Under the action of forces and moments it happens quite often that the coefficients of the deflection curve of the beam is unknown. A deflection curve of a beam can be written in the form

$$v_c = \sum_{i=1}^{n} a_i f_i(x) \tag{4.1}$$

Usually we can find most of the coefficients of the deflection curve using the boundary conditions acting on the beam. However, one of the coefficients is unknown, which we can find that using the Rayleigh's energy approach.

To illustrate the idea, we start with a simple example. The following equations though are not the results for simulating *blunt dissection* but help build up the basic concept needed later.

Let us consider a beam with uniform loading denoted by *q(x)*. As shown in the figure 4.1 below if we consider a small element *dx*, the force acting on the element is given by *q(x)dx*. Considering that the beam deflects in the positive *y* direction by $v_c(x)$, the total work can be evaluated as

$$W_q = \frac{1}{2}\int_0^L q(x)v_c(x)dx \tag{4.2}$$

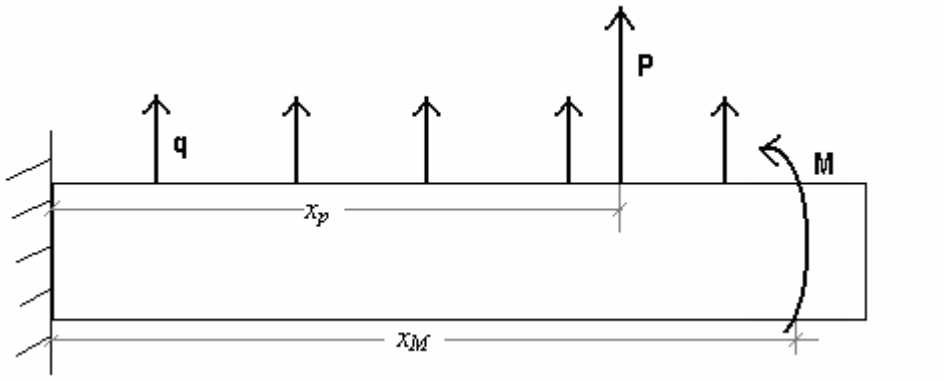

Fig 4.1 Beam under the action of distributed force (q), concentrated force (P) and moment (M)

Besides the distributed load we can also have concentrated load as in our application of *blunt dissection*. The work done due to a concentrated load can be simply evaluated as

$$W_p = \frac{1}{2}P\left[v_c(x)\right]_{x=x_p} \tag{4.3}$$

where *P* is the concentrated load acting at a distance of x_p along the horizontal direction.

For a concentrated moment M, the total work would be

$$W_M = \frac{1}{2} M \left[\frac{dv_c(x)}{dx} \right]_{x=x_M} \tag{4.4}$$

where the slope of the beam $\frac{dv_c(x)}{dx}$ is evaluated at $x = x_M$

After calculating the work done due to distributed load, concentrated load and moment, we need to determine the amount of bending energy that is stored in the beam due to bending. The bending energy of the beam can be determined as [3]

$$U_B = \frac{EI_z}{2} \int_0^L \left(\frac{d^2 v_c}{dx^2} \right)^2 dx \tag{4.5}$$

After evaluating the total work done due to the concentrated load, the distributed load and the moment and the bending energy, we can equate them to find one of the unknown coefficients in $\{a_i\}$ which finally will help determine the deflection in the beam under the action of different forces and moments. Thus, we have

$$W_p + W_q + W_M = U_B \tag{4.6}$$

The solution obtained using the above method is only approximate in nature and, its accuracy depends on how closely the assumed shape matches the actual shape. Also, the assumed shape must meet all the boundary conditions of the beam.

4.2 Rayleigh's energy method applied to beams with axial loading

In section 4.1 we did not consider the effect of axial loading. We focused on the effect of transverse loading on beam. When an axial load (N) acts on the beam accurate results are complex and difficult to derive. In these cases, Rayleigh's [3] has suggested

an approximate way of calculating the deflection curvature introducing the concept of coupling effect.

This concept can be well illustrated using the following example. In figure 4.2 assume that there is an axial force *N* acting on the end of the un-deformed beam *AB*.

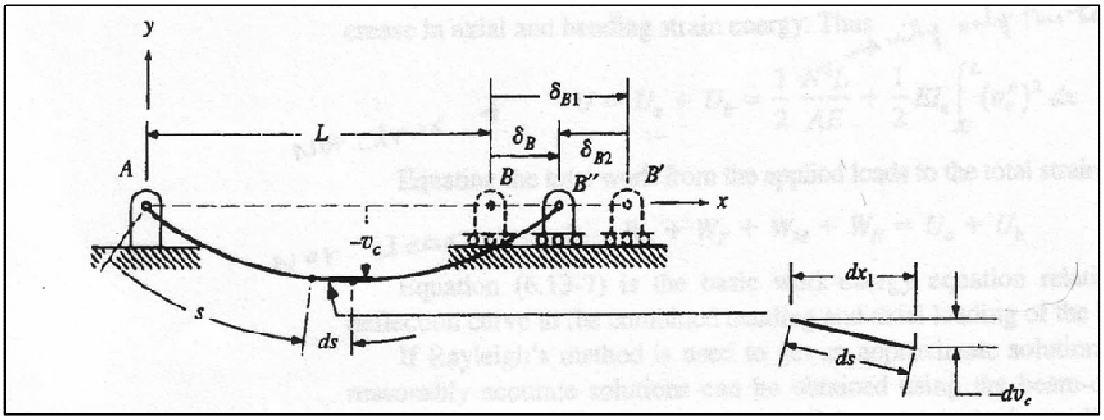

Fig 4.2 Beam undergoing both axial and transverse loading [3]

Rayleigh first considered the axial stretching of the beam due to this axial force *N* such the beam expanded in the longitudinal direction by δ_{B1} to the point *B'*. After that assume a transverse force is applied to the middle of the beam which brings about the bending in the beam causing it to move from point *B'* to *B"* by a distance δ_{B2} as shown in figure 4.2. This distance multiplied by the axial force gives the coupling effect (W_{CN}) between bending and axial force *N*. Thus, the modified total work done (W_N) to axial force *N* can be written as

$$W_N = \frac{1}{2}\frac{N^2 L}{AE} - N\delta_{B2} \tag{4.7}$$

where

$$W_{CN} = N\delta_{B2} \tag{4.8}$$

and

$$\delta_{B2} = \int ds - \int dx = \int dx\left[1 + \left(\frac{dy}{dx}\right)^2\right]^{1/2} - \int dx = \int_0^L \left[\left[1 + \left(\frac{dy}{dx}\right)^2\right]^{1/2} - 1\right] dx \tag{4.9}$$

Rayleigh's approach can therefore be used for axial forces by incorporating the effect of equation 4.7 in equation 4.6. Thus, this approach comes very handy in simulating *blunt dissection,* where we have some axial force acting on the beam as will be discussed in chapter 5. The concept of coupling between axial and transverse force is very significant in our application.

CHAPTER 5

MATHEMATICAL MODELING FOR BLUNT DISSECTION

5.1 Mathematical foundation for calculating deflection

In this section and the following sections, we describe our original work of deriving a beam model to simulate an organ. We start with a hypothetical beam (see figure 5.1 below) on which the total force is equal to *2P* acting at the center in the transverse direction. The beam represents a duct – like organ and *2P* represents the force exerted by a grasper in the hands of a surgeon. Also the length of the beam is assumed to be *2L*.

As can been be seen from figure 5.1, since the beam is symmetric about its

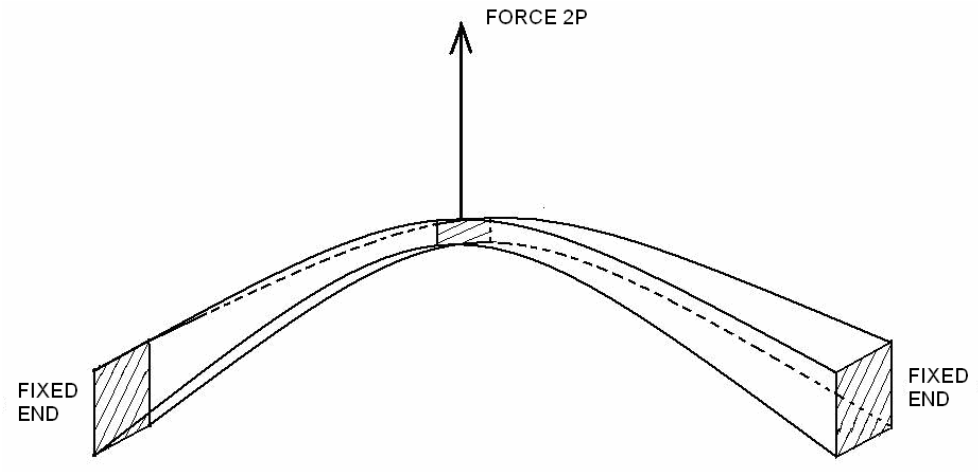

Fig. 5.1 A simple beam undergoing large deflection

center both in terms of boundary conditions and geometry, we can work with one half of the beam for the derivation (see figure 5.2 below). This is a standard practice in Civil and Mechanical Engineering.

Thus, in figure 5.2, the beam is anchored at the left end denoted by *A*. The other end is free to move in the transverse direction under the action of force *P* (due to symmetry one-half of the total force is considered). The term v_c denotes the vertical deflection of the beam at a particular position *x* of the beam. This is the deflection that we are interested in calculating and, in real life would represent the deflection of the organ due to grasping and pulling.

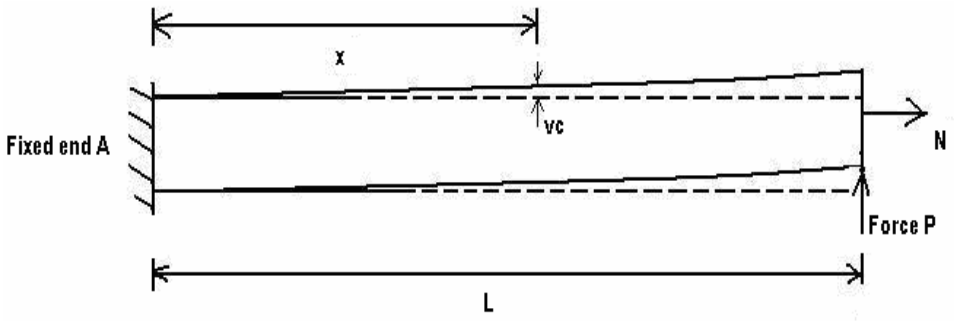

Fig. 5.2 Left half of the beam.

We can now examine some of the boundary conditions that will aid in deriving a mathematical equation to calculate the deflection. Firstly, the deflection at the point *A* can be taken to be zero, since it is fixed. Also, the slope at *A* is clearly zero (always true for cantilever type beams). As we are working with one-half of the beam due to the symmetry, the slope at the right end of the beam segment turns out to be zero. Taking into account these boundary conditions, we start with an assumed deflection curve and

determine its coefficients by using these boundary conditions and the Rayleigh's energy method [3].

In the following derivations, we assume a cubic curve for the vertical deflection (v_c) of the beam. The equation of the curvature can therefore be written as

$$v_c = a_0 + a_1 x + a_2 x^2 + a_3 x^3 \tag{5.1}$$

where v_c is the vertical displacement at a distance x from the origin and a_0, a_1, a_2 and a_3 are the constants to be determined.

This is a well understood assumption in Civil Engineering [3]. This model is also feasible for the following practical reasons. Firstly, in this cubic curve (see equation 5.1), we have four unknowns. Three of these unknowns can be determined using the boundary conditions stated above. We will then be left with one unknown which can be determined using the Rayleigh's energy method [3].

5.1.1. Application of boundary conditions

We have both vertical displacement and slope equal to zero at $x = 0$, hence we evaluate both a_0 and a_1 to be zero.

$$\text{at } x = 0, v_c = 0 \Rightarrow a_0 = 0 \tag{5.2}$$

$$\text{at } x = 0, \frac{dv_c}{dx} = 0 \Rightarrow a_1 = 0 \tag{5.3}$$

The third boundary condition, we have that the slope at $x = L$ is equal to zero. Therefore

$$\text{at } x = L, \frac{dv_c}{dx} = 0 \Rightarrow 2a_2 L + 3a_3 L^2 = 0$$

$$\Rightarrow a_3 = -\frac{2a_2}{3L} \tag{5.4}$$

Substituting for a_0, a_1 and a_3 in equation 5.1, we have

$$v_c = a_2(x^2 - \frac{2x^3}{3L}) \tag{5.5}$$

5.1.2. Rayleigh's energy method

It may be recalled that the basic principle of Rayleigh's energy method is to equate the total external work done on the beam to the total internal strain energy stored in the beam. We can calculate the work done due to transverse force P (see equation 5.8), the coupling effect of the axial force W_{CN} (see equation 5.16) and the strain energy due to bending (see equation 5.20). We can now solve for a_2 by the Rayleigh's energy approach using the following equation.

$$W_p + W_A - W_{CN} = U_B + W_A \tag{5.6}$$

Knowing a_2, we can determine the deflection of the beam at any position x given a transverse force P.

5.1.3. Work done by force P

The total work done due to force P is given by

$$W_P = 0.5Pv_c \tag{5.7}$$

In figure 5.2, the force P acts at the end of the beam i.e. at $x = L$. Therefore we have

$$W_p = \left[\frac{1}{2} P a_2 (x^2 - \frac{2x^3}{3L}) \right]_{x=L}$$

$$= \frac{1}{6} L^2 P a_2 \tag{5.8}$$

5.1.4. Work done by force N

The normal force *N* as described in figure 5.2 is dependent on the amount of stretching the beam undergoes due to applied transverse load *P*. We can describe the effect of this normal force in terms of work done as the sum of two components, the work done due to axial stretching W_A and its coupling effect with that of the bending [3] which increases with deflection. Since we are equating the external work done to the internal strain energy, we need not find the work done W_A explicitly as the term will appear on both sides of the equation. The other term due to coupling effect needs to be calculated as this term only appears in the work done side and doesn't contribute to internal energy. The total work done due to normal force *N* can thus be derived as the following equation:

$$W_N = W_A - qN \int_0^L \left[\left\{ 1 + \left(\frac{dv_c}{dx} \right)^2 \right\}^{\frac{1}{2}} - 1 \right] dx \tag{5.9}$$

where *q* is a factor used to account for the influence of *N* in computing the work, which we will discuss in detail later in this section. The second term in equation 5.9 involving the integral is an approximate value for the coupling effect W_{CN}. W_{CN} is essentially the work done by the normal force *N* due to the bending effect. The value of *N* is determined using the following relation (see figure 5.3) [1]

$$N = \frac{AE}{L} dl \tag{5.10}$$

For a small slope the work done due to coupling effect can be evaluated using the following step:

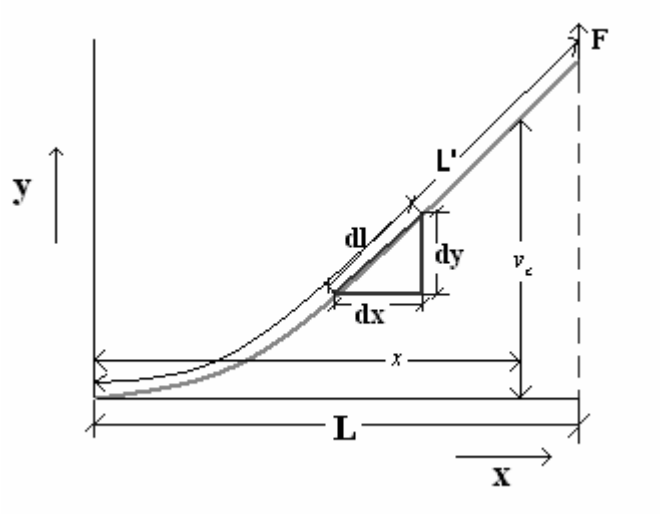

Fig. 5.3 Calculation of *N*

After deflection and the resulting stretching, the new length of the beam *L'* can be obtained as

$$L' = \int dl = \int_0^L \left(\sqrt{1 + \left(\frac{dv_c}{dx} \right)^2} \right) dx \tag{5.11}$$

For a small slope $\frac{dv_c}{dx} << 1$, equation 5.11 can therefore be simplified to the case

$$L' = \int dl = \int_0^L \left(1 + \frac{1}{2} \left(\frac{dv_c}{dx} \right)^2 \right) dx \tag{5.12}$$

where only the first order Taylor series expansion term is retained.

Change in length of the beam like tissue is given by

$$\Delta l = L' - L = \int_0^L \frac{1}{2}\left(\frac{dv_c}{dx}\right)^2 dx \tag{5.13}$$

where from equation 5.5, we have

$$\frac{dv_c}{dx} = 2a_2\left(x - \frac{x^2}{L}\right) \tag{5.14}$$

Substituting equation 5.14 in equation 5.13, we have

$$\begin{aligned}\Delta l &= \int_0^L \frac{1}{2} 4{a_2}^2 \left[x - \frac{x^2}{L}\right]^2 dx \\ &= 2{a_2}^2\left[\frac{L^3}{3} + \frac{L^3}{5} - \frac{L^3}{2}\right] \\ &= \frac{{a_2}^2 L^3}{15}\end{aligned} \tag{5.15}$$

Therefore, the coupling energy is derived as

$$W_{CN} = qN\int_0^L \left[\left\{1 + \left(\frac{dv_c}{dx}\right)^2\right\}^{\frac{1}{2}} - 1\right] dx = q\frac{AE}{L}\left(\frac{{a_2}^2 L^3}{15}\right)^2 \tag{5.16}$$

The parameter q plays a vital role in making this mathematical model work for comparatively large deflection. It is observed that for a small deflection range we need to take q as 1.0 because the change in N is comparatively small for small deflections. But as we increase the transverse force and hence the deflection, a value of between 0.5 ~ 0.4 is found to work well. This is explained in greater detail in chapter 7. Correct

selection on the value of q gives us a beam model results that has the same accuracy as a detailed *FEM* model.

5.1.5. Strain energy due to bending

Now we evaluate the internal energy stored in the beam due to bending. This denoted by U, was shown in chapter 4 as:

$$U = \frac{1}{2EI_z}\int_0^L M_z{}^2 dx \tag{5.17}$$

Once again, we assume the slope to be small which implies $\frac{dv_c}{dx} << 1$

Even when the slope is small, the deflections can be large. In equation 5.6 we have assumed more bending energy than the actual bending energy with this approximation. On the other hand the coupling energy (W_{CN}) is assumed to be less than what it would be in reality. So even with the assumption of small slope our derivation works well even for larger deflections *as the extra bending energy considered compensates the less coupling energy considered.* This qualitative statement will be backed with quantitative numbers in chapter 7.

Now, we calculate the total bending energy as

$$U_B = \frac{EI_z}{2}\int_0^L \left(\frac{d^2 v_c}{dx^2}\right)^2 dx \tag{5.18}$$

$$\frac{d^2 v_c}{dx^2} = 2a_2\left(1-\frac{2x}{L}\right) \tag{5.19}$$

Substituting equation 5.19 into equation 5.18 we can derive bending energy as

$$U_B = \frac{EI_z}{2}\int_0^L \frac{4a_2^2(L^2 + 4x^2 - 4xL)}{L^2}dx$$
$$= \frac{2a_2^2 EI_z}{L^2}(L^3 + \frac{4L^3}{3} - 2L^3)$$
$$= \frac{2a_2^2 EI_z L}{3} \qquad (5.20)$$

5.1.6. Strain energy due to axial stretching

The strain energy stored due to axial stretching is same as W_A. This helps us finding the coefficient a_2 without determining W_A. This is because the same term appears both in the work done and the strain energy and hence is not required to determine a_2.

5.2 Correction for shear energy

The vertical displacement does depend on the shear forces but the magnitude of effect is function of the aspect ratio (ratio of length to the diameter of the beam). For long, thin beams (large aspect ratio) the effect is negligible as compared to the case of short thick beam (smaller aspect ratio)[2]. Since we are essentially working with a large aspect ratio in our application, we have not considered the effect of shear. However, we can now consider its effect and make the necessary corrections to equation 5.6. For very thin beams under very large deflection, we have proposed to neglect the bending effect of the beam and simply formulated the deflection using the axial stretching as described in the following section 5.3.

5.3 Mathematical model for very large deflection with larger aspect ratio

For very large deflection and for thin diameters, the bending effect of the beam is negligible compared to that of axial stretching (see figure 5.4). In this case, we can ignore the curvature and represent the beam with straight lines.

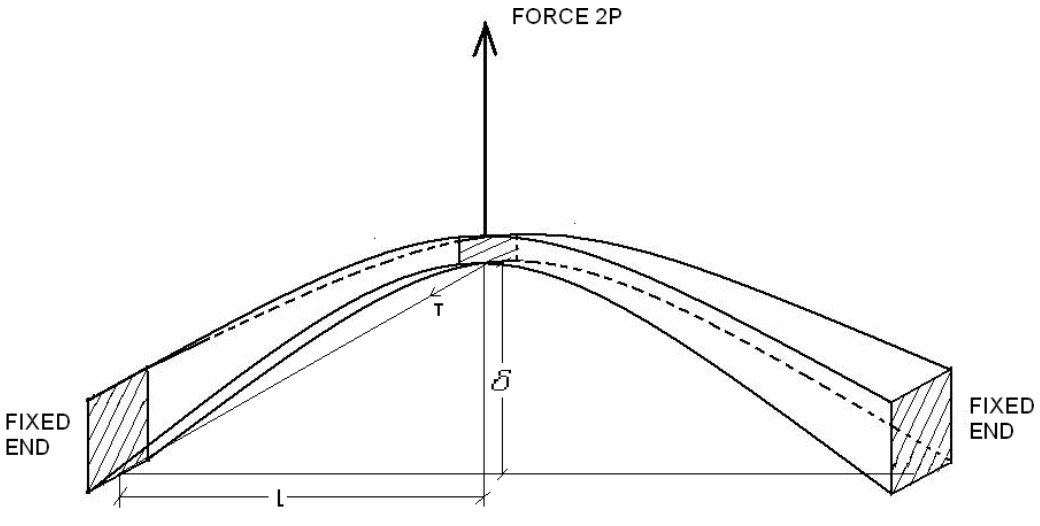

Fig. 5.4 Beam model for very large deflection and large aspect ratio.

The spring constant of the beam can be derived as

$$k = \frac{AE}{L} \tag{5.21}$$

The relation between the tension T in the beam and the applied transverse force P is given by the following equation (see figure 5.4)

$$T = \frac{P\sqrt{L^2 + \delta^2}}{\delta} \tag{5.22}$$

The change in length is given by

$$\Delta l = \sqrt{(L^2 + \delta^2)} - L \tag{5.23}$$

Therefore considering only axial stretching, we have

$$T = k\Delta l = k\left(\sqrt{(L^2 + \delta^2)} - L\right) \tag{5.24}$$

Equating equations 5.22 and 5.24, we can find the load displacement curve for large deflection. The final relationship can be derived as

$$P = k\delta\left[1 - \frac{L}{\sqrt{(L^2 + \delta^2)}}\right] \tag{5.25}$$

5.4 Blunt Dissection

The videos that we obtained for *blunt dissection* clearly revealed that the *bile duct* ruptured under the action of a large axial and bending force [24]. We used this observation to set thresholds for axial and bending forces needed for rupture of the simulated organ.

The total axial strain can be formulated as

$$\varepsilon_a = \frac{\Delta l}{L} \tag{5.26}$$

Where $\Delta l = L' - L$ and can be calculated using equation 5.13.

Therefore, the normal stress σ_N can be evaluated using isotropic organs as

$$\sigma_N = E\varepsilon \tag{5.27}$$

Also the total bending stress σ_B can be evaluated using the flexure formula [3], which is also a well known equation in Civil engineering.

$$\sigma_B = \frac{M_Z c}{I_z} \tag{5.28}$$

where *c* is the maximum surface distance from the neutral axis of the beam.

Hence *blunt dissection* (see figure 5.5) takes place when

$$\sigma_N + \sigma_B > \mathrm{T} \tag{5.29}$$

where T is the threshold force value for the dissection to take place.

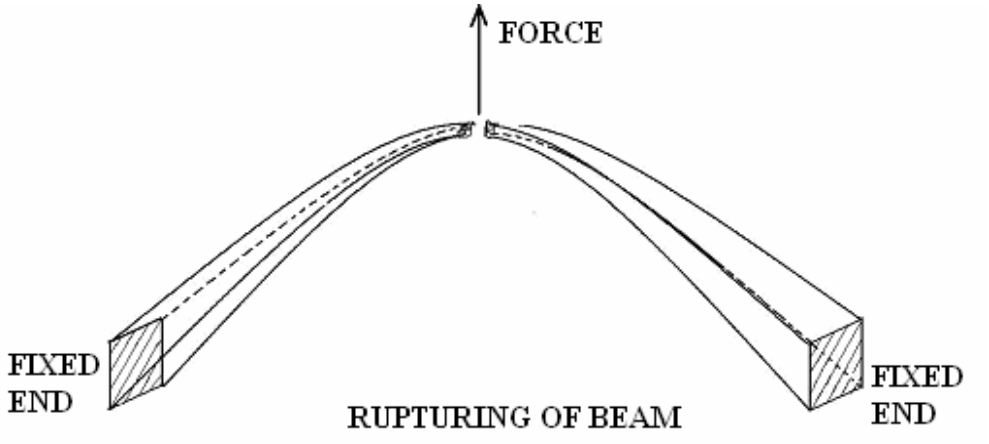

Fig. 5.5 Blunt Dissection

In addition to the normal stress a bending stress is acting on the cross sectional area. This bending stress is at its highest value at the surface of the duct. The *bile duct* will therefore, first tear at the surface.

CHAPTER 6

VALIDATION OF A PROPOSED BEAM MODEL AGAINST FEM

In this chapter, we perform a validation of the proposed beam model. We assume the beam model can represent a long and tubular organ. Therefore, the material properties such as the Young's modulus and Poisson ratio are chosen to match such an organ. Thereafter, the deflections of such an organ are calculated using the equations derived so far for the beam. Simultaneously, the same organ is modeled using an FEM approach. This is typically performed by inputting appropriate parameters into a well known FEM program called ANSYS. ANSYS requires that we specify the number of elements, material properties and whether or not linear or non – linear analysis should be used. In our case, due to the nature of the deflection, non – linear analysis is the correct choice.

6.1 Comparison of deflections between *Beam Model* and *FEM* for rubber like material with large aspect ratio

We first applied our model to simulate deflections in a material which behaves like rubber. For the typical simulation results below, the length of the half -beam is taken to be *1 inch*, diameter *0.4 inch*, Young's modulus as *1500 psi (corresponding to rubber)*, Poisson ratio *0.3* and for different values of *P*. The deflection at $x = 1$ inch is compared between our method (*Beam Model*) and *FEM* – the non real time gold standard for accuracy.

The finite element analysis was performed using 40 beam elements. The largest error corresponds to the high load is approximately 9.5% between beam model and FEM model (see Table 6.1).

Table 6.1 Percentage error in deflection for rubber like organ with large aspect ratio

Diameter = 0.4inch, E = 1500psi			
Force (lbs)	Deformation calculated (Beam Model) (inch)	Deformation actual (FEM) (inch)	% Error
0	0	0	0.00%
1	0.043976852	0.0437	0.63%
2	0.086520266	0.085	1.79%
3	0.126605275	0.123	2.93%
4	0.163749542	0.157	4.30%
5	0.197897743	0.187	5.83%
6	0.22923599	0.215	6.62%
7	0.258048918	0.24	7.52%
8	0.284638504	0.264	7.82%
9	0.309286683	0.285	8.52%
10	0.332242075	0.306	8.58%
11	0.35371814	0.324	9.17%
12	0.373896019	0.342	9.33%
13	0.392928869	0.359	9.45%
14	0.410946283	0.376	9.29%
15	0.428058269	0.391	9.48%
20	0.502895775	0.461	9.09%

In figure 6.1, we illustrate side by side the deflections obtained for the beam and FEM (simply a plot version of the table).

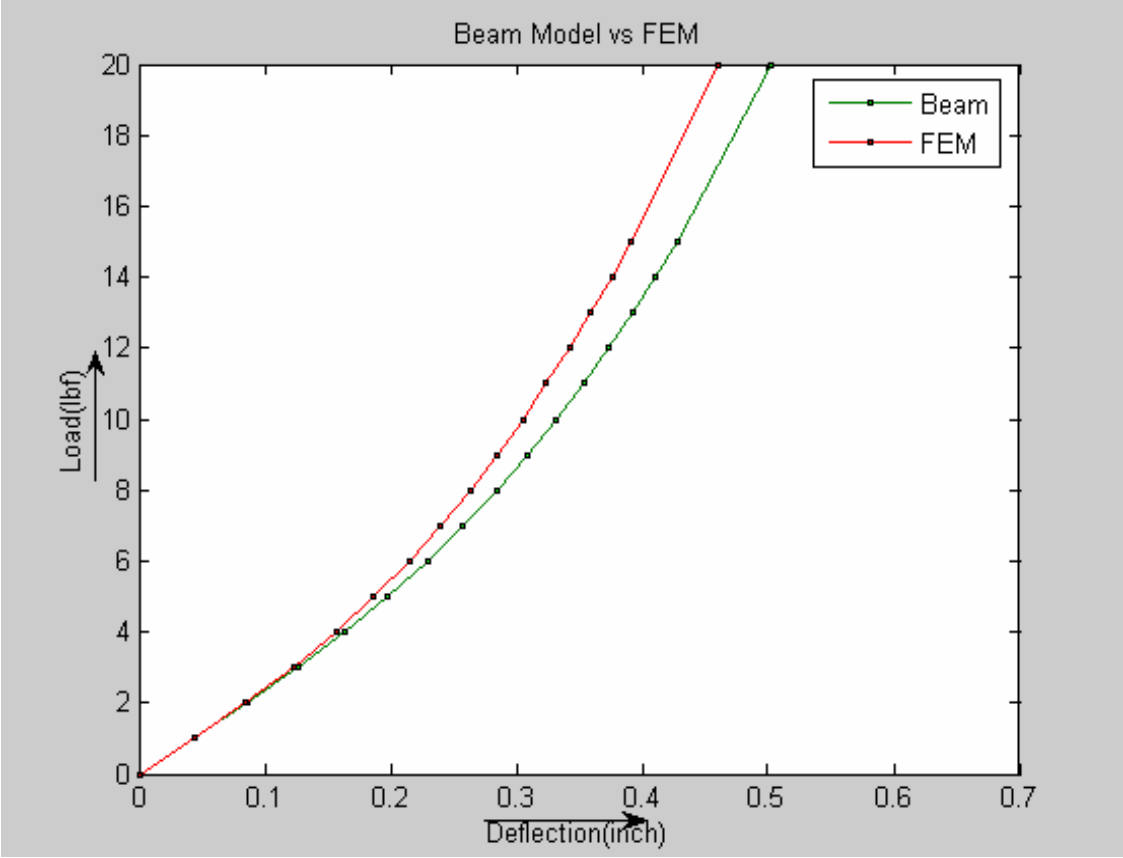

Fig 6.1 Load Deflection curve for *Beam Model* vs. *FEM* for organ having rubber like property

It should be pointed out that our modeling efforts are geared towards providing a sense of touch (haptic effect) to the surgeon performing the surgery. A 10% difference between what a surgeon would feel in a simulator versus what he is supposed to feel in actual surgery is unlikely to be an issue. Mass spring models, presently used to provide such feedback could be off by as much as 100%.

6.2 Some screen shots from *ANSYS* for section 6.1

Figure 6.3 illustrates a typical output of the ANSYS code that generates the FEM model. In this case *P* is equal to *5 lbf*. Non – linear analysis is used. DMX is the deflection. The same nomenclature is followed for the rest of the snapshots shown hereafter.

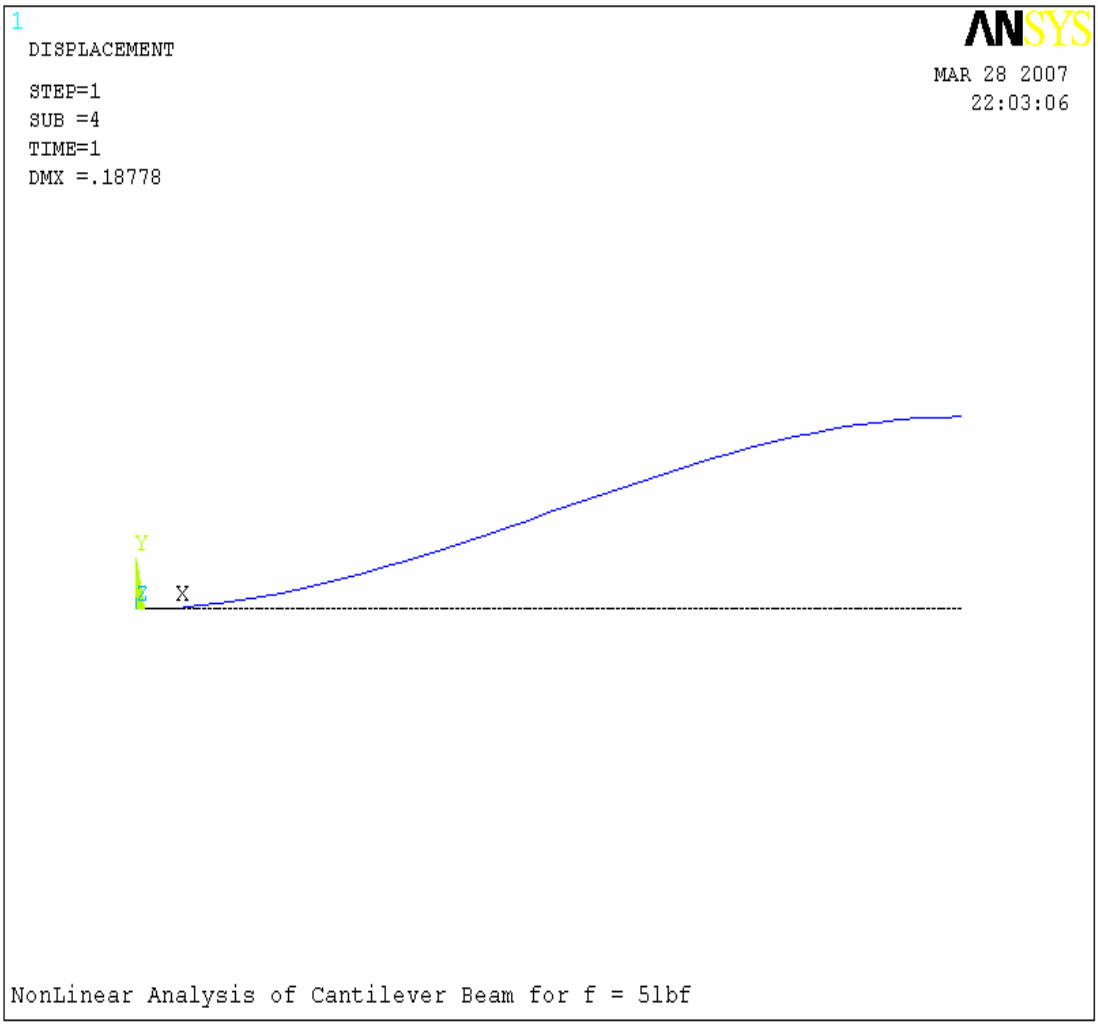

Fig 6.2 Force is equal to 5 lbf

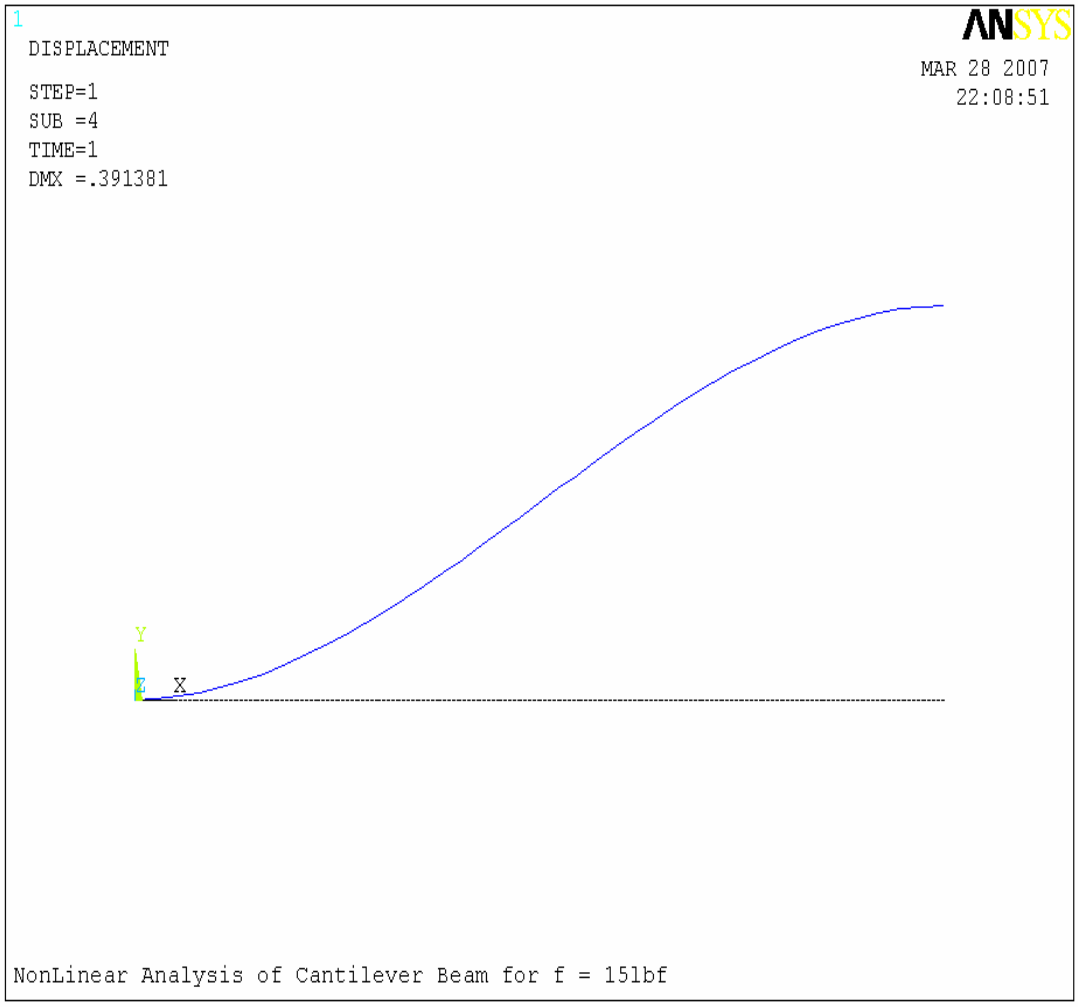

Fig 6.3 Force is equal to 15 lbf

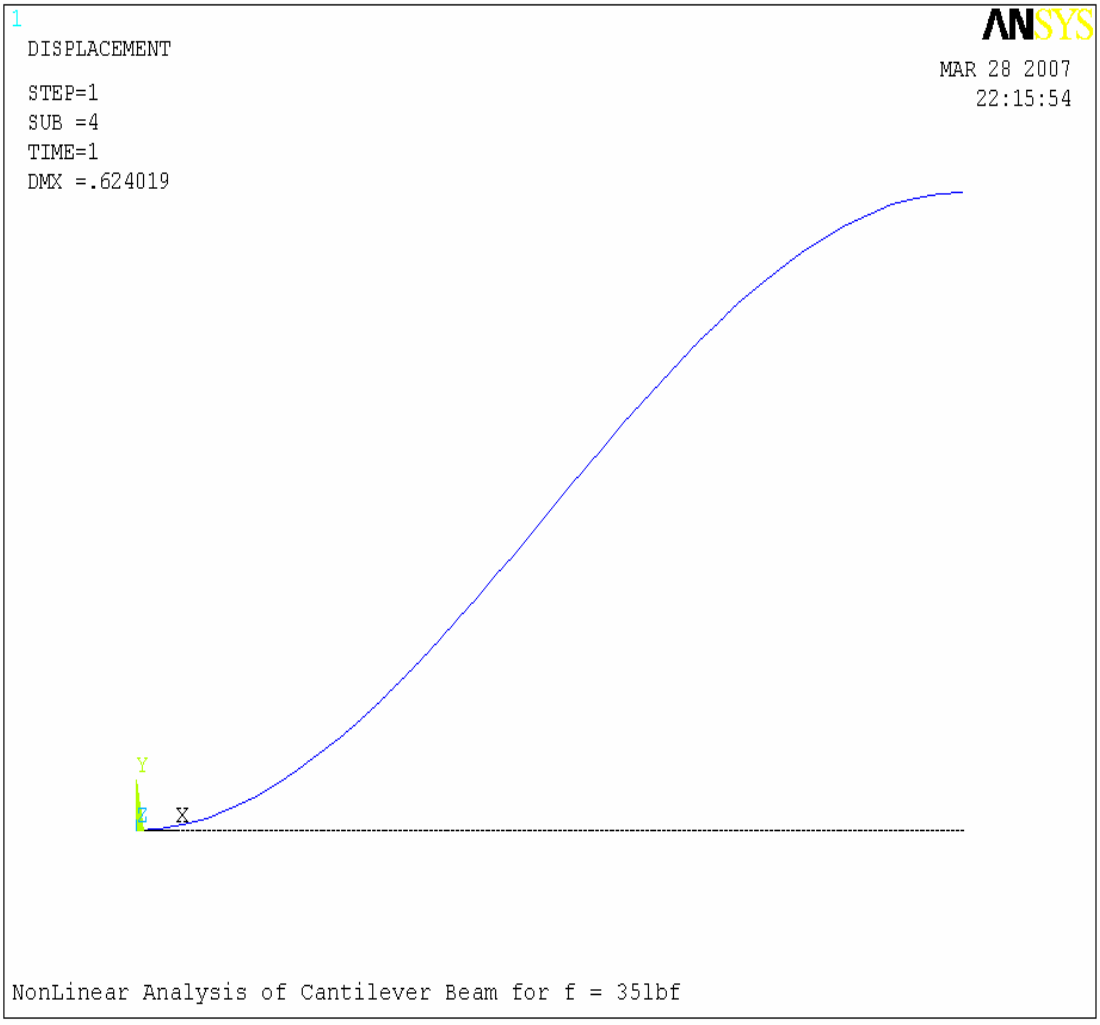

Fig 6.4 Force is equal to 35 lbf

6.3 Comparison of large deflections between *Beam Model* and *FEM* for rubber like material having very thin diameter and large aspect ratio

For very thin beams and a large aspect ratio with material properties same as that of a rubber (as considered in section 6.1), we modeled the organ neglecting the bending effect as described in section 5.3. We took the diameter as *0.1 inch* in this case with all other parameters the same as section 6.1. We compared the results with *FEM* and our approach had a maximum error of 7.22%.

Table 6.2 Percentage error in deflection for thin and very long organ having rubber like property

Force (lbf)	Deformation calculated (inch)	Deformation actual (inch)	% Error
0	0	0	
1	0.598314452	0.558	7.22%
2	0.78934952	0.748	5.53%
3	0.939278779	0.896	4.83%
4	1.070192942	1.025	4.41%
5	1.189988135	1.14	4.38%

6.4 Some screen shots from ANSYS for section 6.3

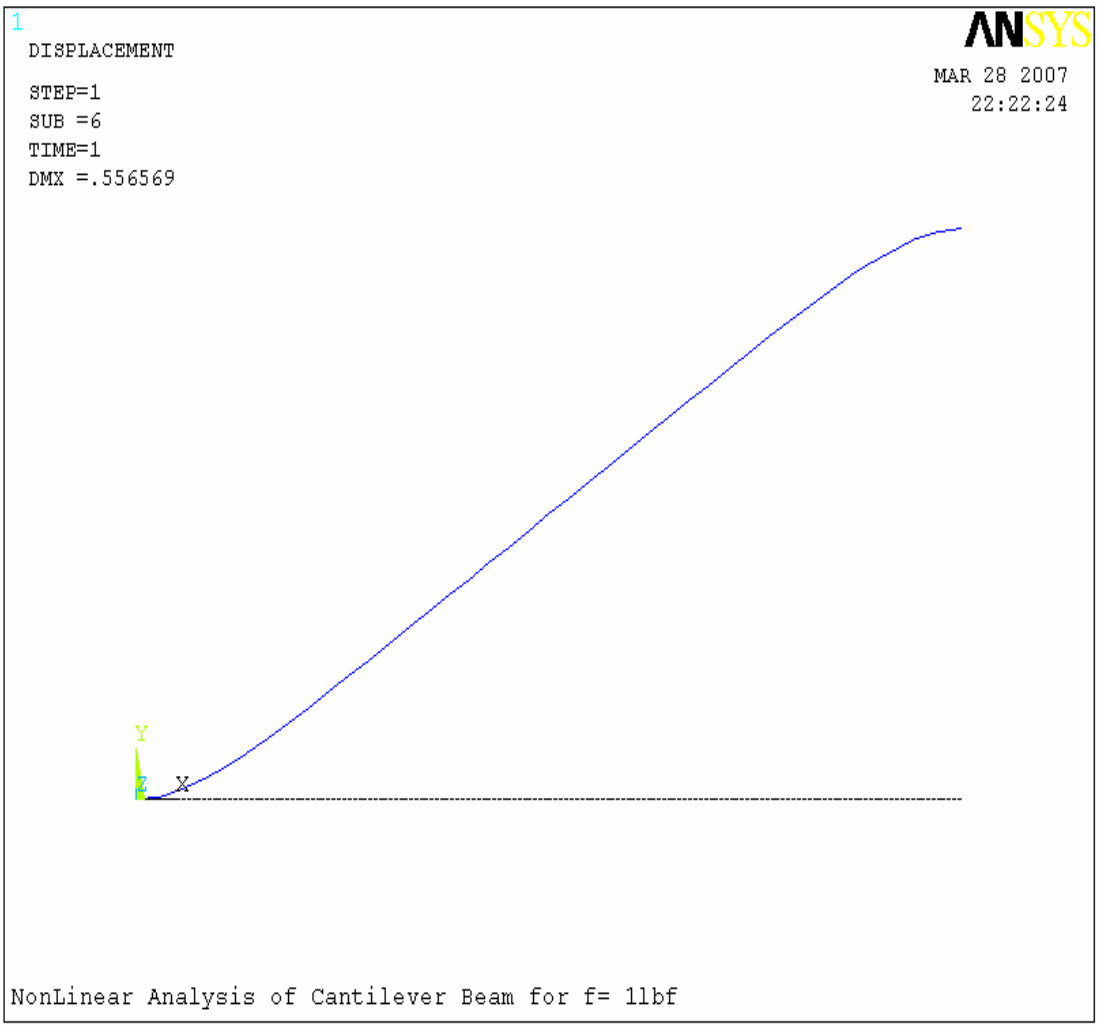

Fig 6.5 Force is equal to 1 lbf

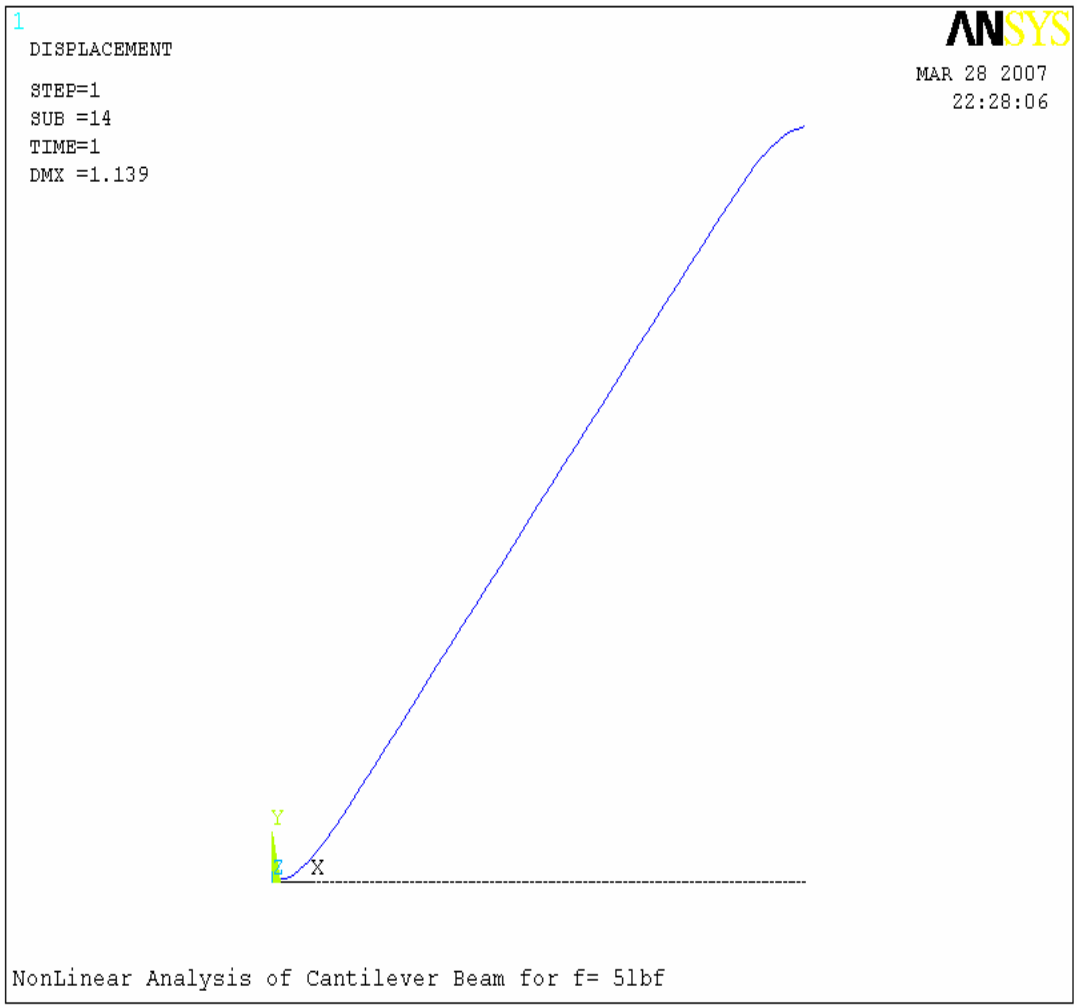

Fig 6.6 Force is equal to 5 lbf

6.5 Results for *blunt dissection* of *bile duct*

We used published data from [15] for the estimation of material properties and dimensions (especially diameter) of a *bile duct* on which the *blunt dissection* is actually being carried out. We found that for this simulation(see Table 6.3 and figure 6.8), we can take the length of the half beam to be *1 inch*, diameter *0.35 inch*, Young's modulus as *45 psi*, Poisson ratio of *0.3*. For different values of P, the deflection at $x = 1$ inch is compared between our method (*Beam Model*) and *FEM*. The finite element analysis once again used 40 beam elements. The maximum error calculated came out to be around *11%*. As already stated in section 5.1.4. , $q = 0.5$ in comparatively large deflection gives satisfactory results.

Table 6.3 Percentage error in deflection between *Beam model* and *FEM* for *bile duct*

Diameter = 0.35inch, E = 45psi			
Force (lbs)	Deformation calculated (inch)	Deformation actual (inch)	% Error
0	0	0	0.00%
0.01	0.025078136	0.02503	0.19%
0.02	0.049796046	0.049433	0.73%
0.03	0.073842132	0.072728	1.53%
0.04	0.096985194	0.094649	2.47%
0.05	0.119082813	0.11511	3.46%
0.06	0.140071203	0.13416	4.41%
0.07	0.159946127	0.1519	5.30%
0.08	0.178742988	0.16845	6.11%
0.09	0.196520337	0.18395	6.83%
0.1	0.213347962	0.19851	7.47%
0.11	0.229299067	0.21223	8.04%
0.15	0.28571136	0.26061	9.63%
0.2	0.343703521	0.31066	10.64%
0.25	0.392167613	0.3532	11.03%
0.3	0.4339643	0.39066	11.08%
0.35	0.470855528	0.42444	10.94%
0.4	0.503987995	0.45543	10.66%
0.45	0.534145741	0.48423	10.31%
0.5	0.561887452	0.51128	9.90%
0.55	0.587625092	0.53687	9.45%
0.6	0.611671212	0.56123	8.99%
0.65	0.63426868	0.58454	8.51%
0.7	0.655610089	0.60695	8.02%
0.75	0.675850841	0.62858	7.52%
0.8	0.695118239	0.64952	7.02%
0.85	0.713517944	0.66985	6.52%
0.9	0.731138674	0.68962	6.02%
0.95	0.748055694	0.70889	5.52%
1	0.764333436	0.72773	5.03%
1.05	0.780027515	0.74616	4.54%
1.1	0.795186292	0.76422	4.05%
1.2	0.824062241	0.79933	3.09%
1.3	0.851243958	0.8333	2.15%
1.4	0.876955181	0.86627	1.23%
1.5	0.901376277	0.89839	0.33%
1.6	0.924654956	0.92973	0.55%
1.7	0.946913839	0.96043	1.41%
1.8	0.968255933	0.99051	2.25%
1.9	0.988768682	1.0201	3.07%
2	1.00852701	1.0492	3.88%
2.5	1.098002171	1.1889	7.65%

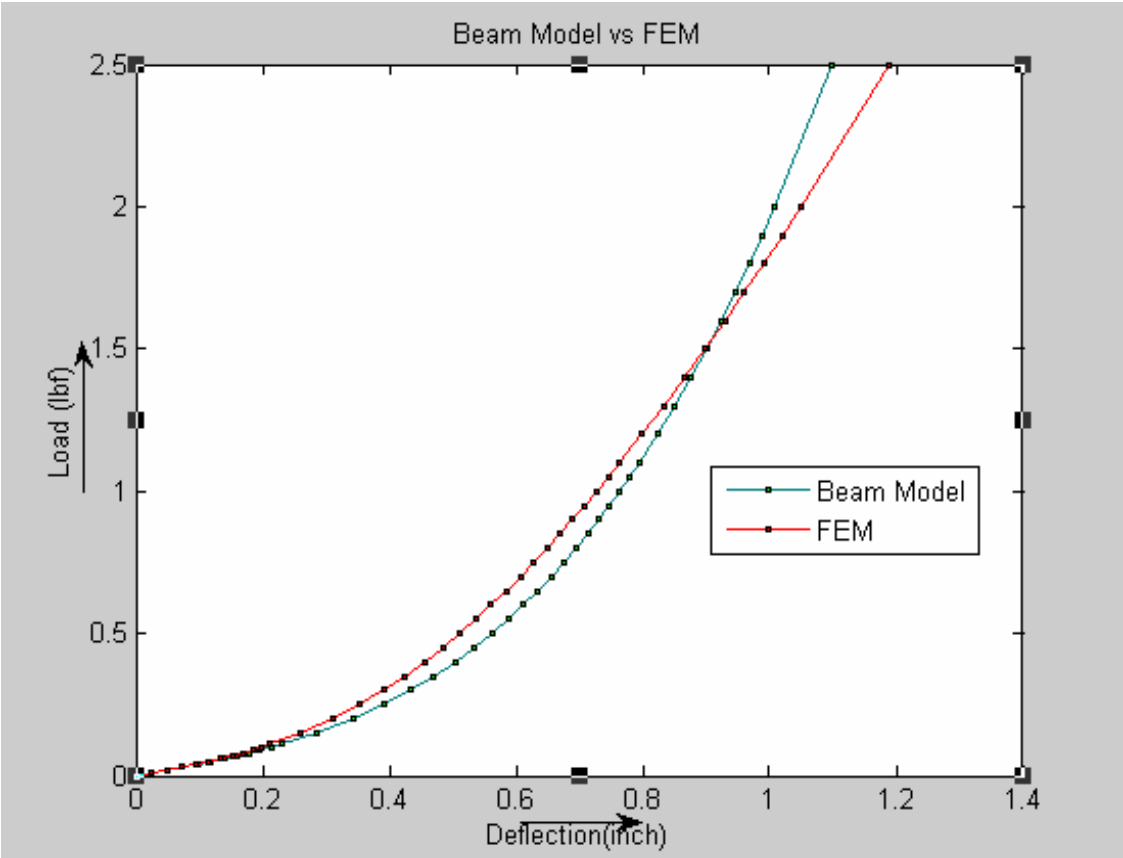

Fig 6.7 Load deflection curve of *Beam Model* vs. *FEM* for *bile duct*

In the following figure 6.9, we have shown the variation of the normal force versus the deflection at the end of the beam. This validates our earlier statement in section 5.1.4, where we took the linear variation of N and chose to work with a value of q between 0.5 ~ 0.4. It is evident from the figure below that the assumption makes sense and, as a result the deflection of beam model follows the FEM results closely in figure 6.8.

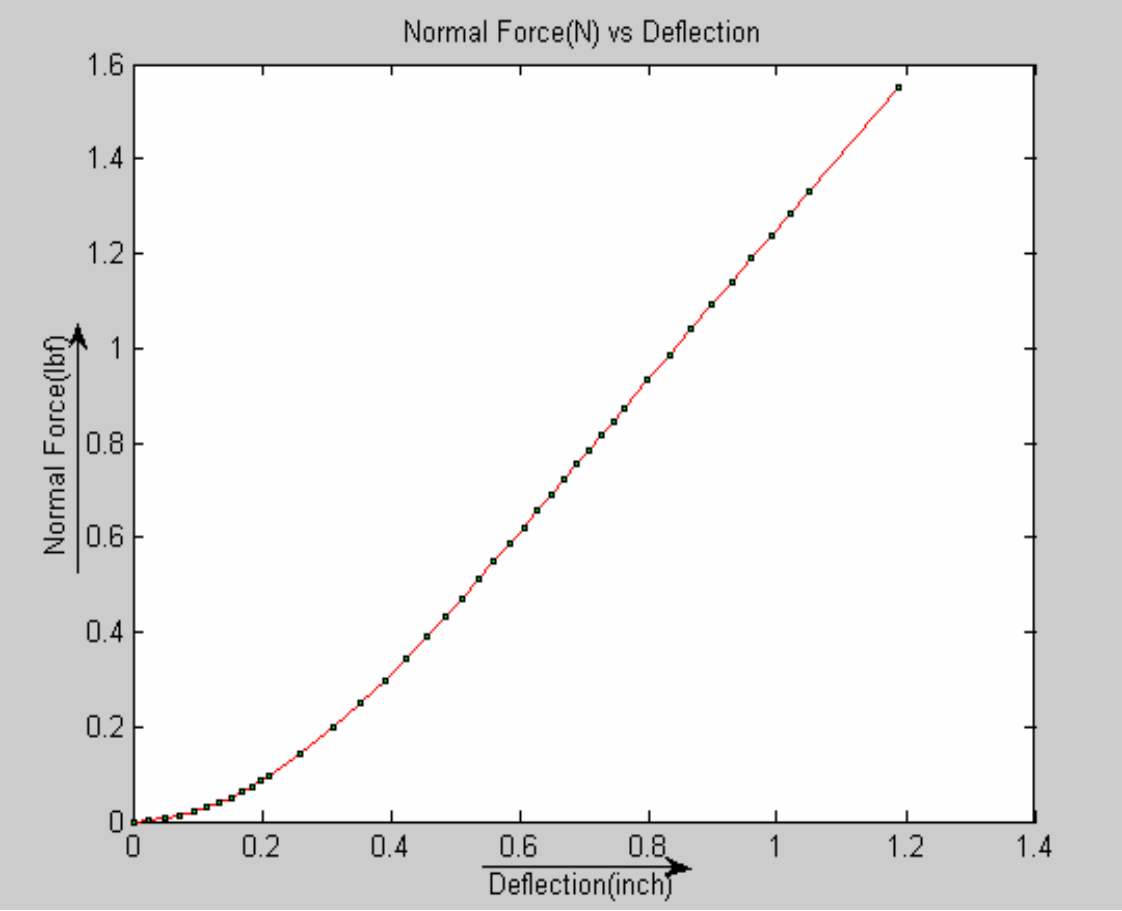

Fig 6.8 Normal force (N) vs deflection curve analysis in *FEM* for $x = L$

6.6 Some screen shots from ANSYS using the properties of *bile duc*t and applying different forces

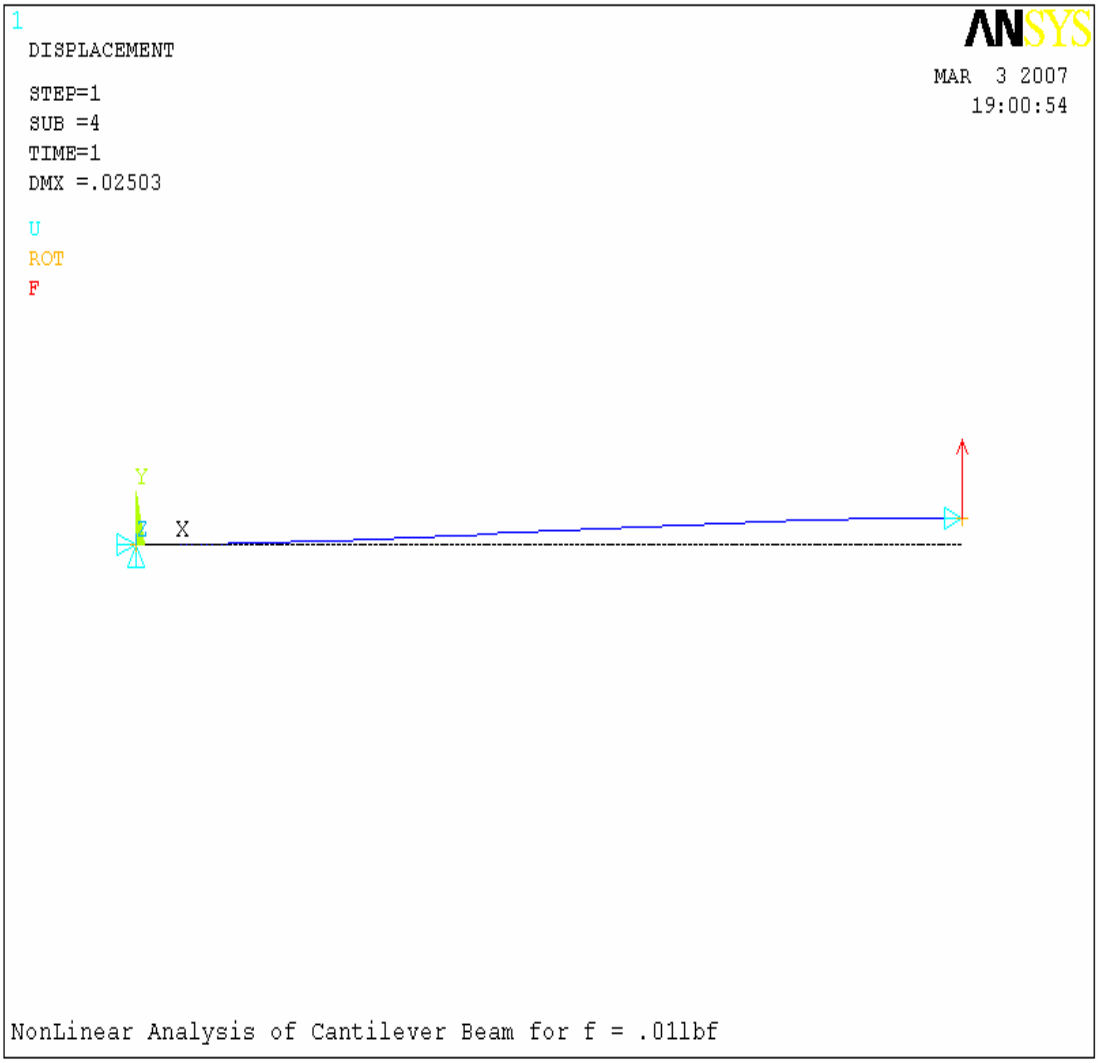

Fig 6.9 Force is equal to 0.01 lbf

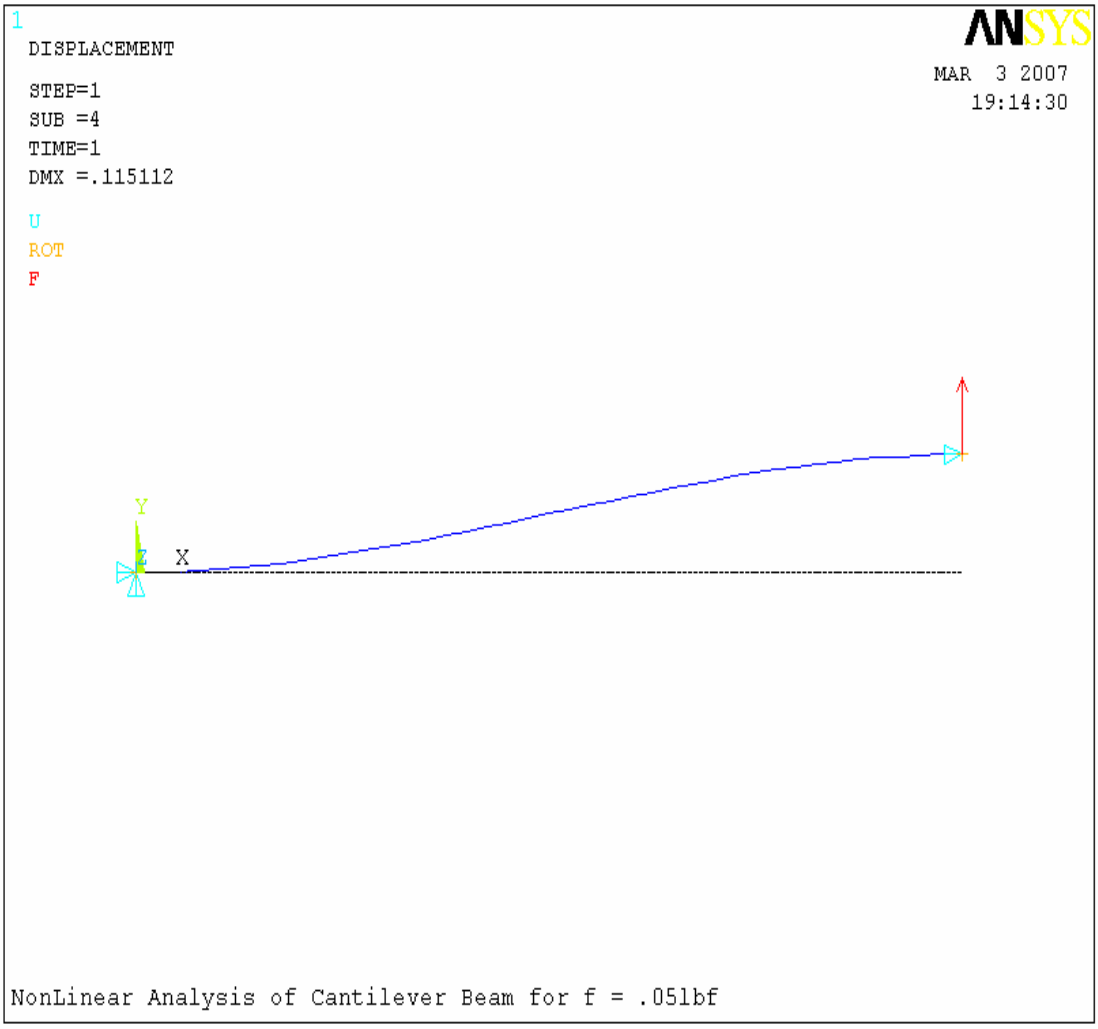

Fig 6.10 Force is equal to 0.05 lbf

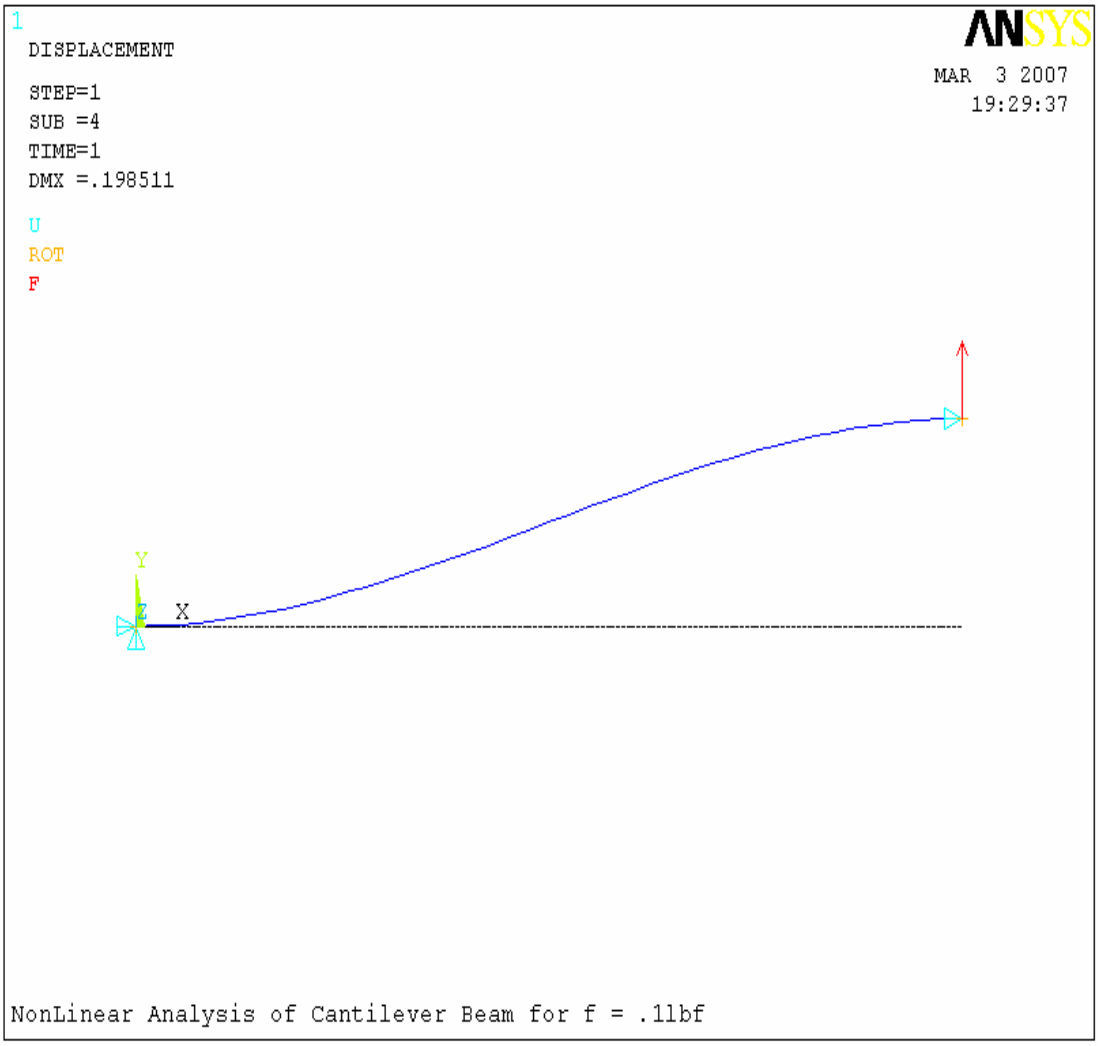

Fig 6.11 Force is equal to 0.1 lbf

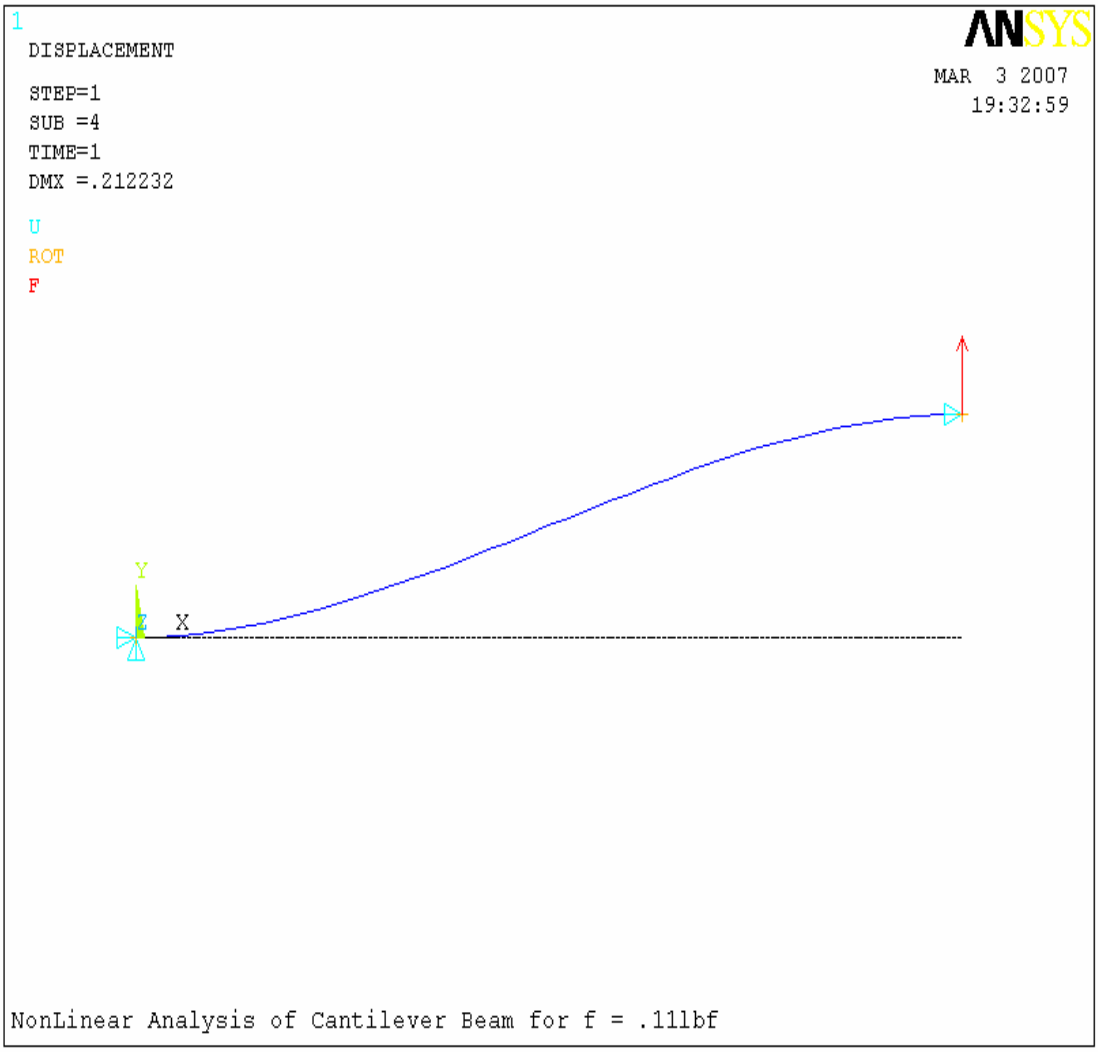

Fig 6.12 Force is equal to 0.11 lbf

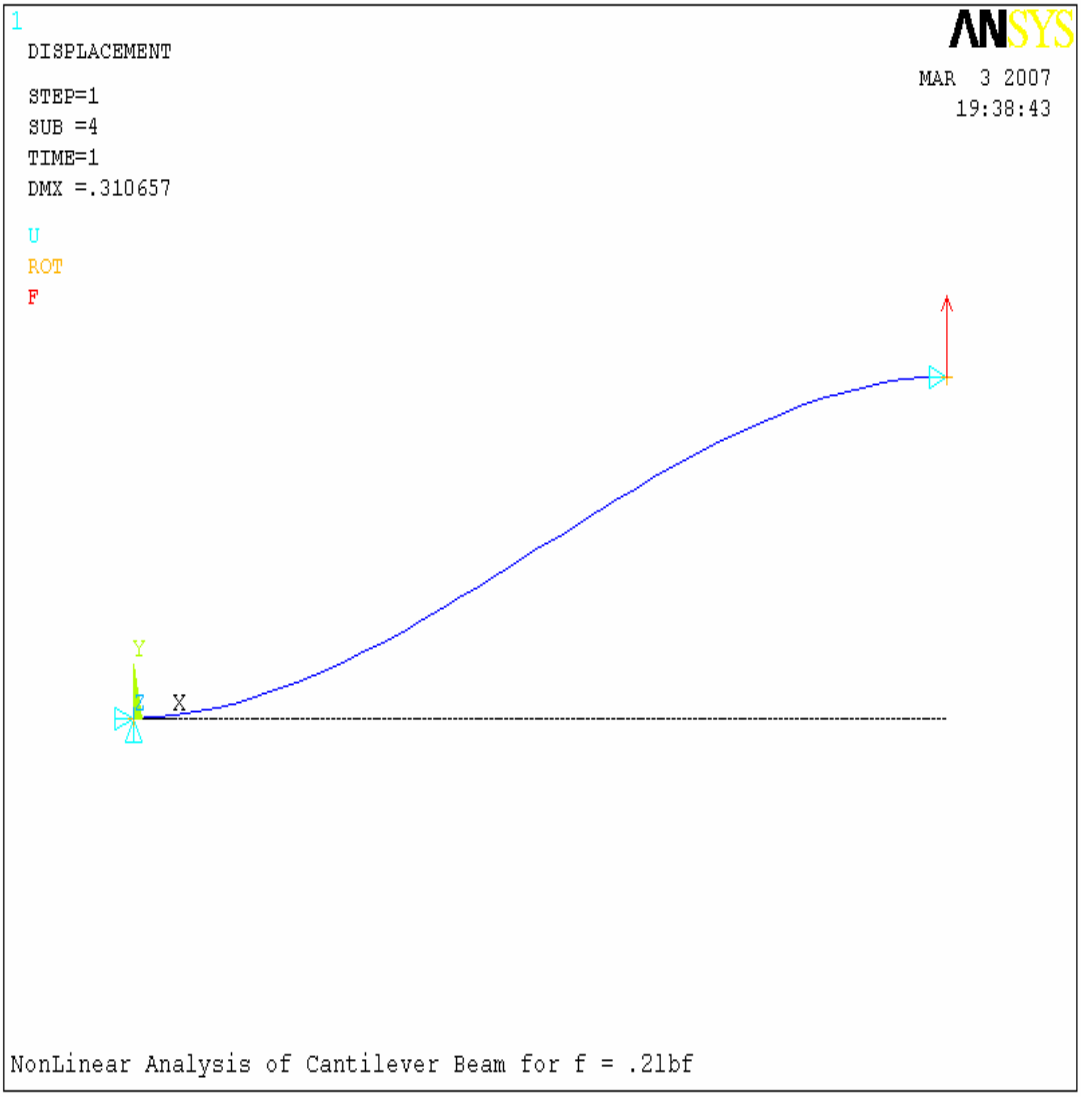

Fig 6.13 Force is equal to 0.2 lbf

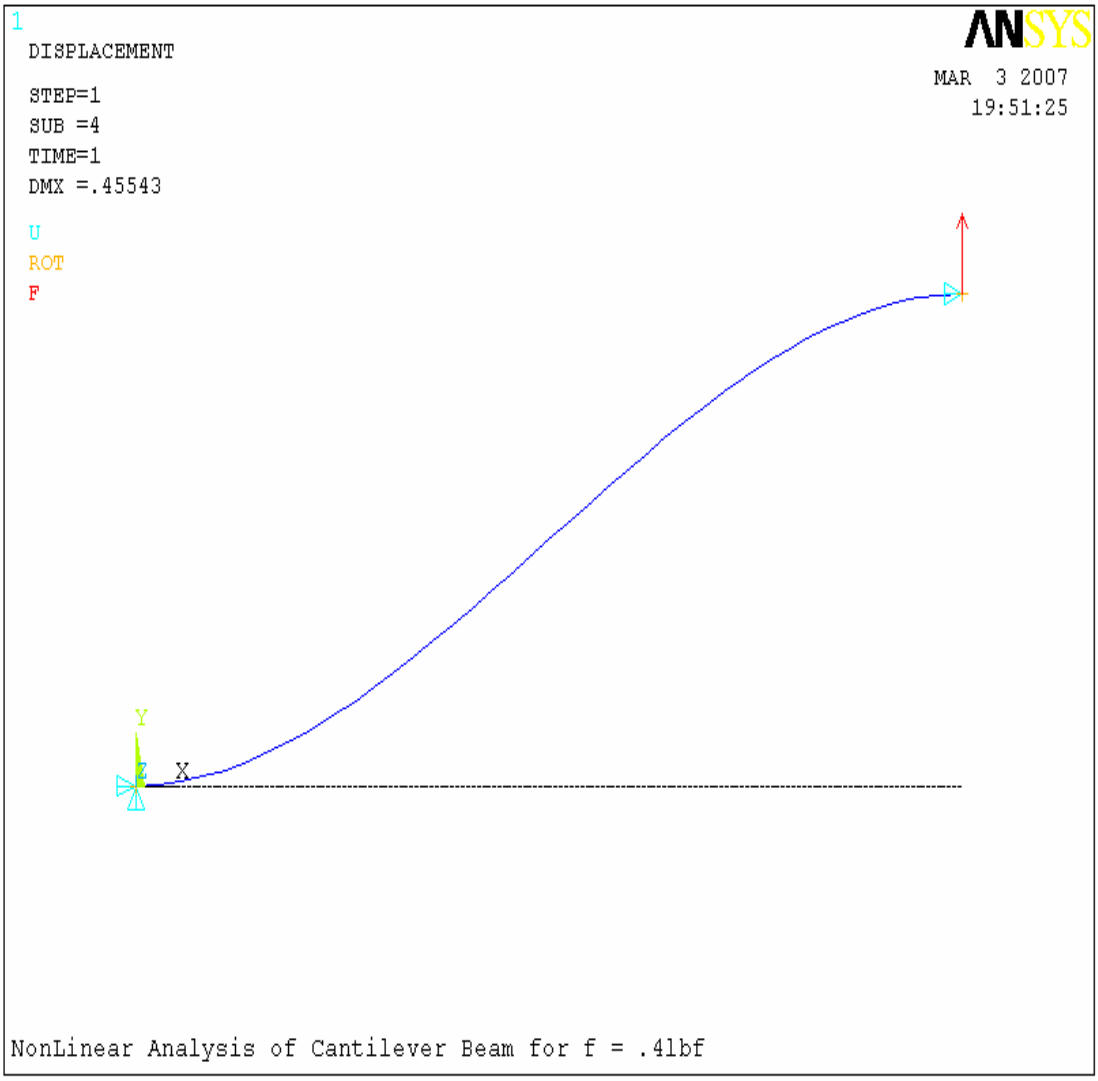

Fig 6.14 Force is equal to 0.4 lbf

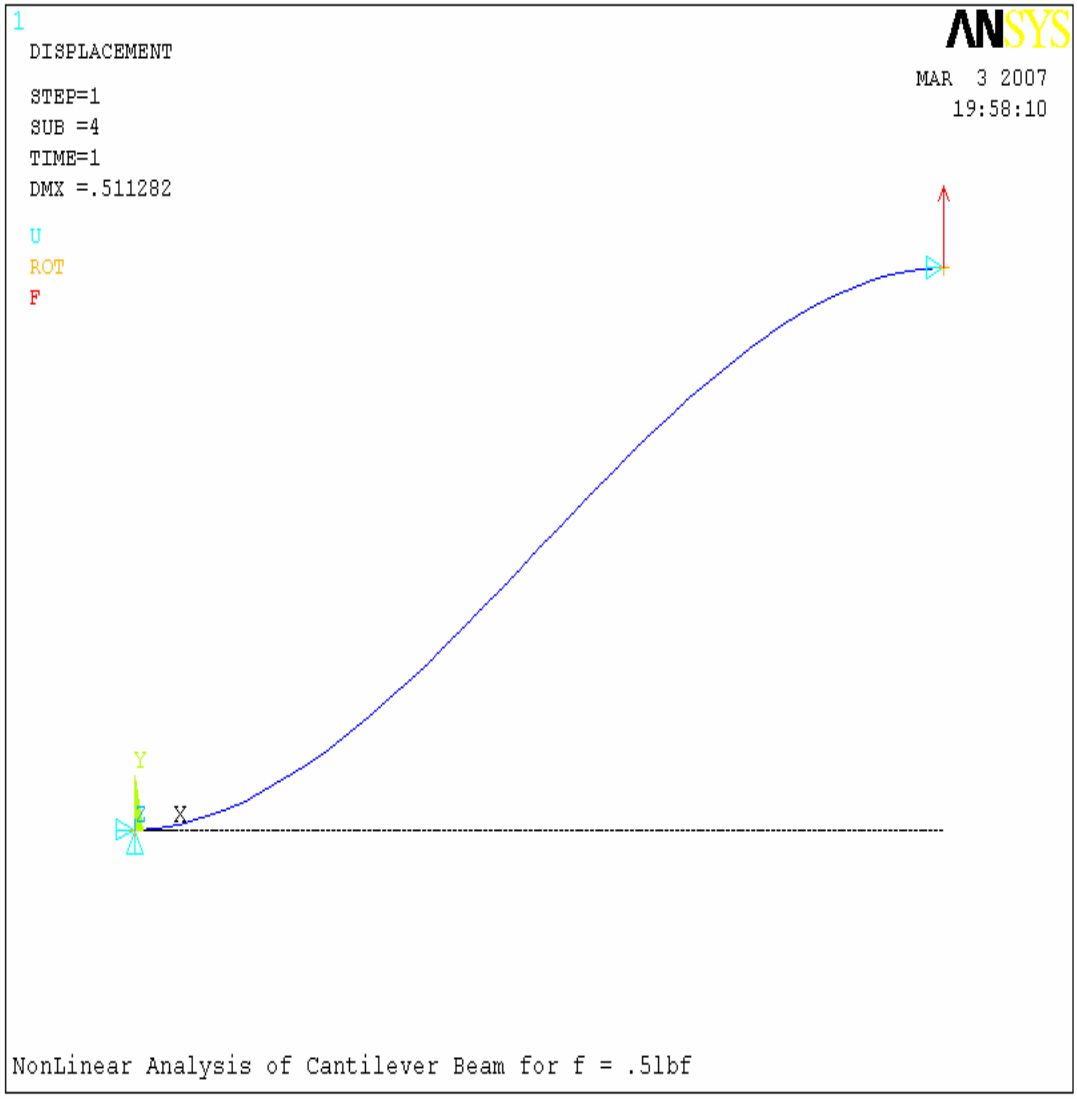

Fig 6.15 Force is equal to 0.5 lbf

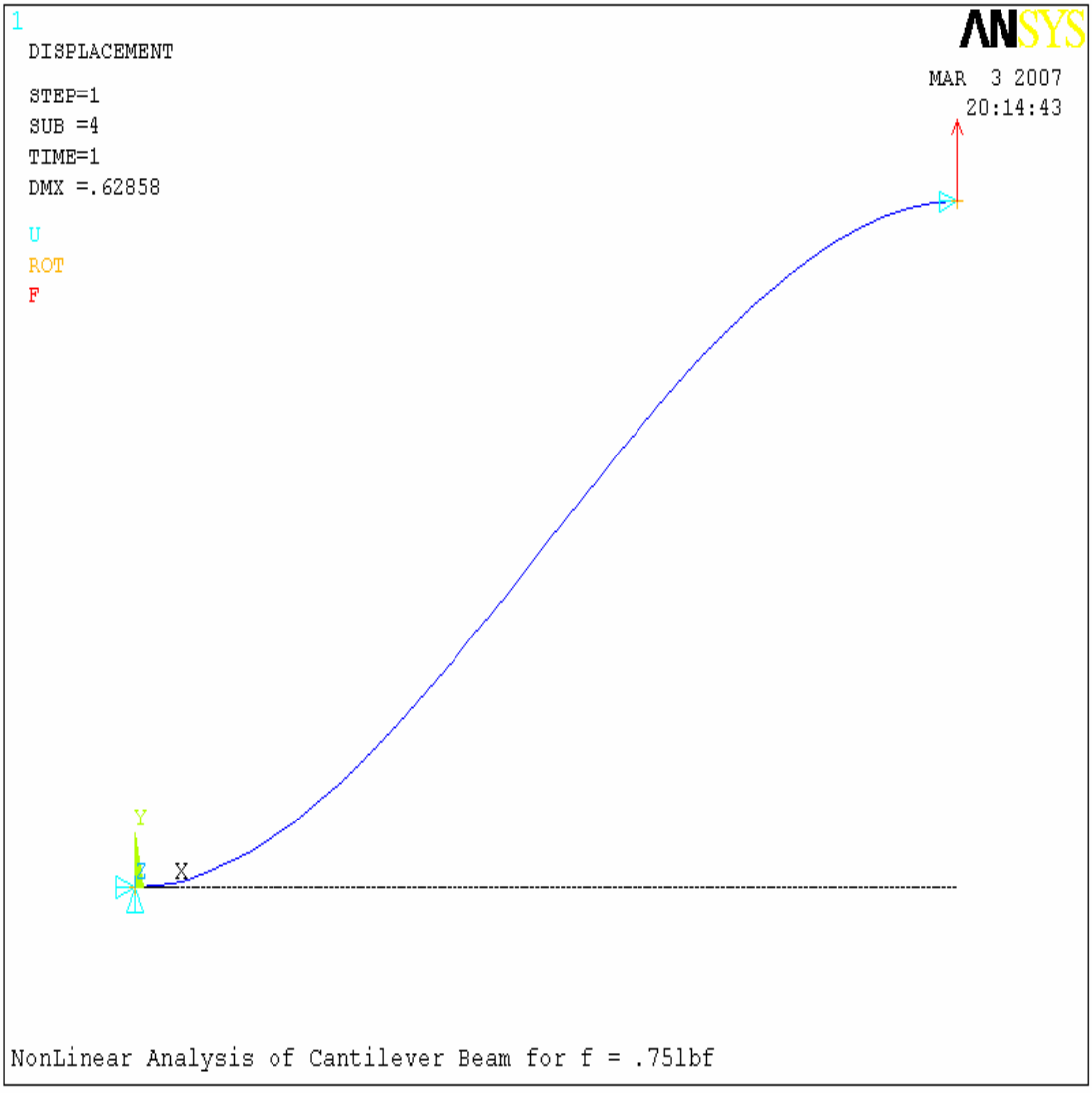

Fig 6.16 Force is equal to 0.75 lbf

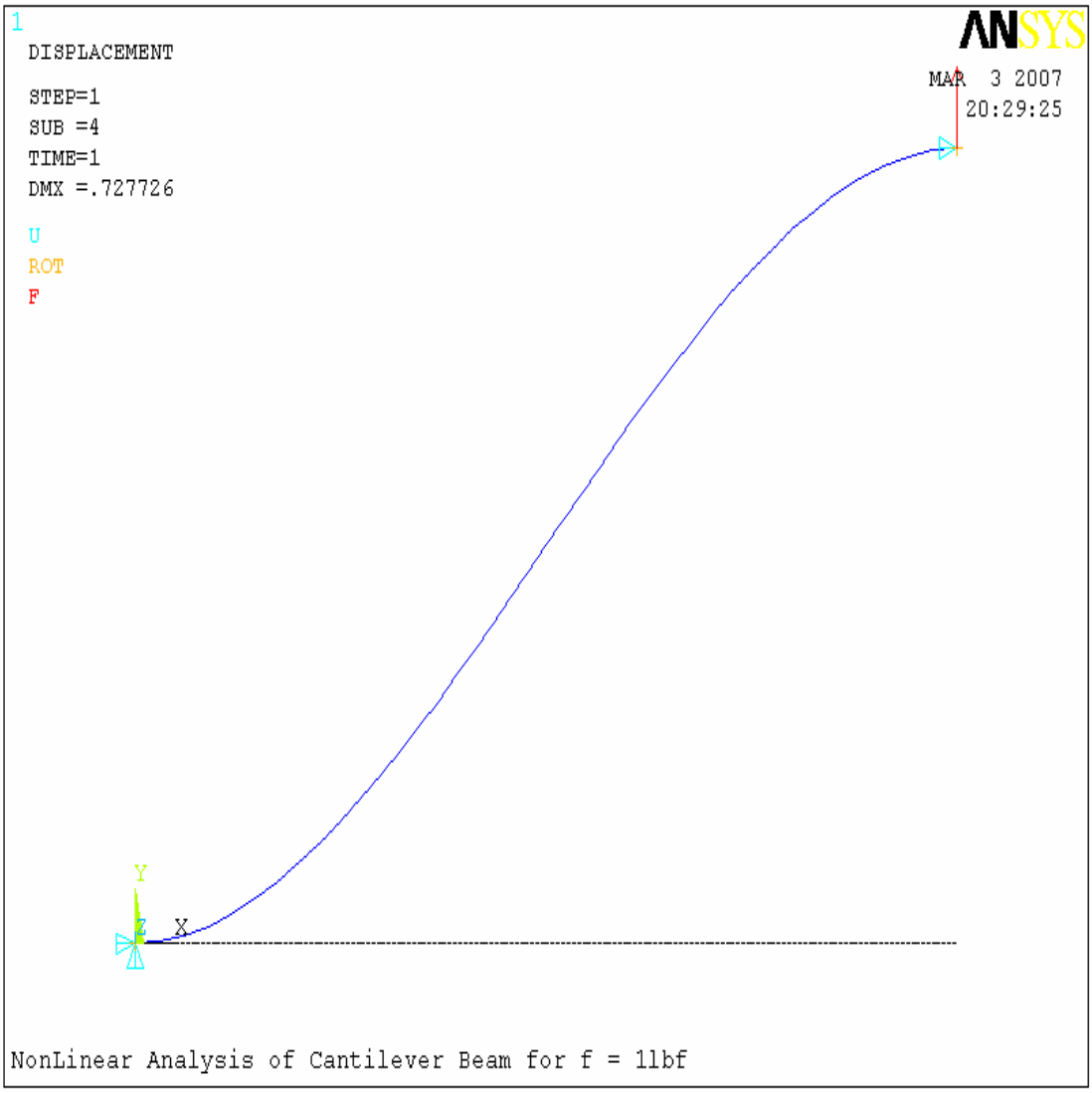

Fig 6.17 Force is equal to 1.0 lbf

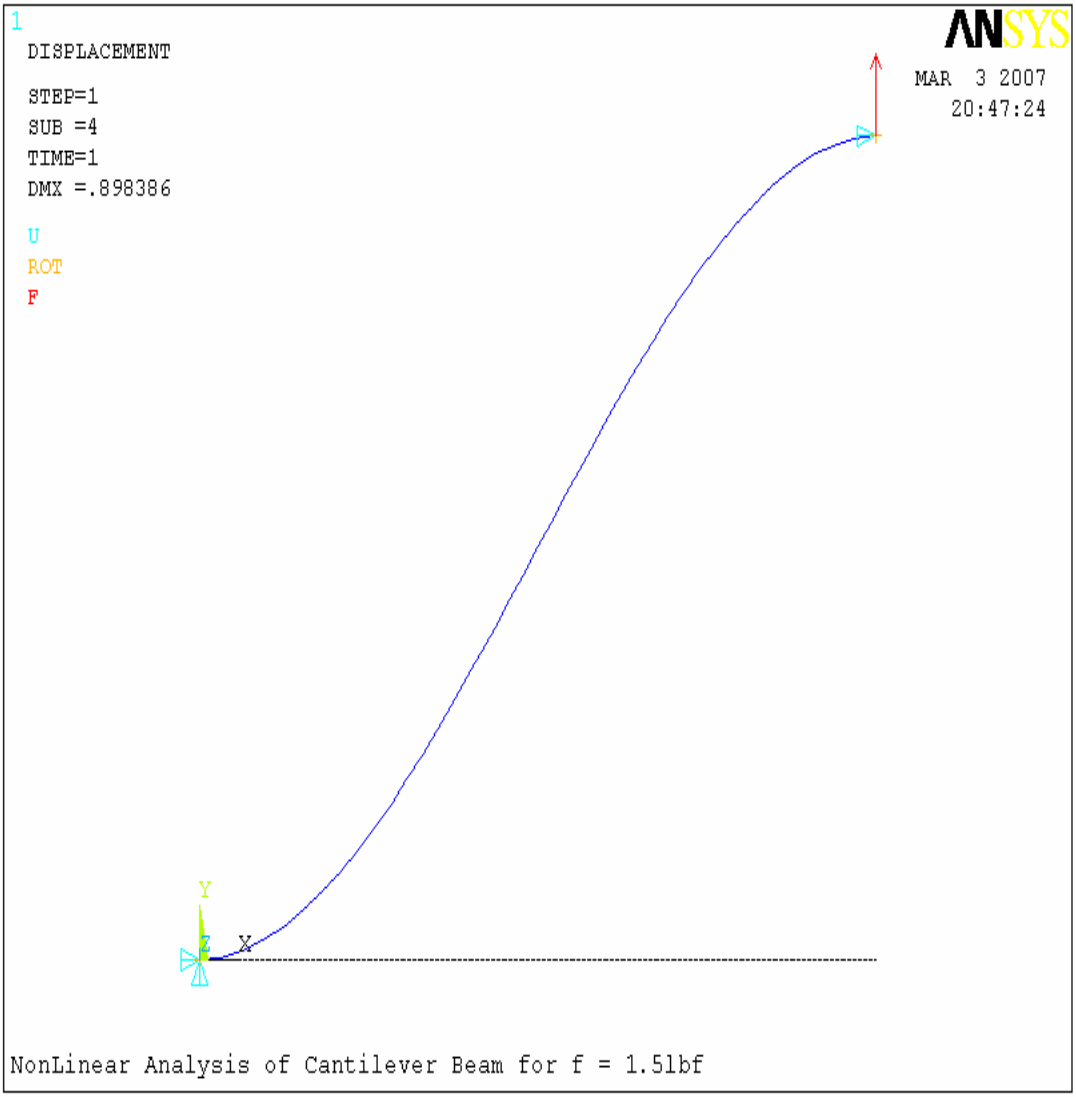

Fig 6.18 Force is equal to 1.5 lbf

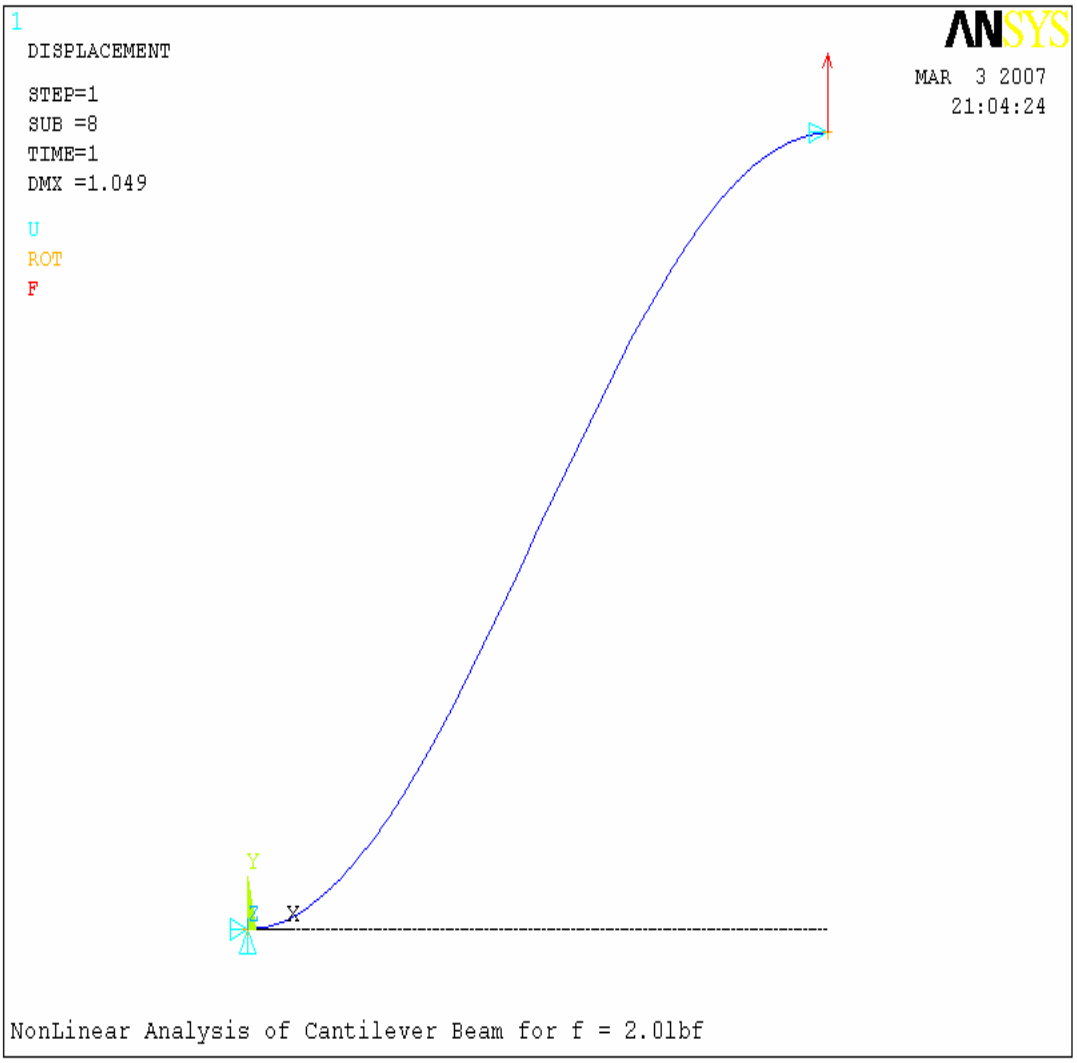

Fig 6.19 Force is equal to 2.0 lbf

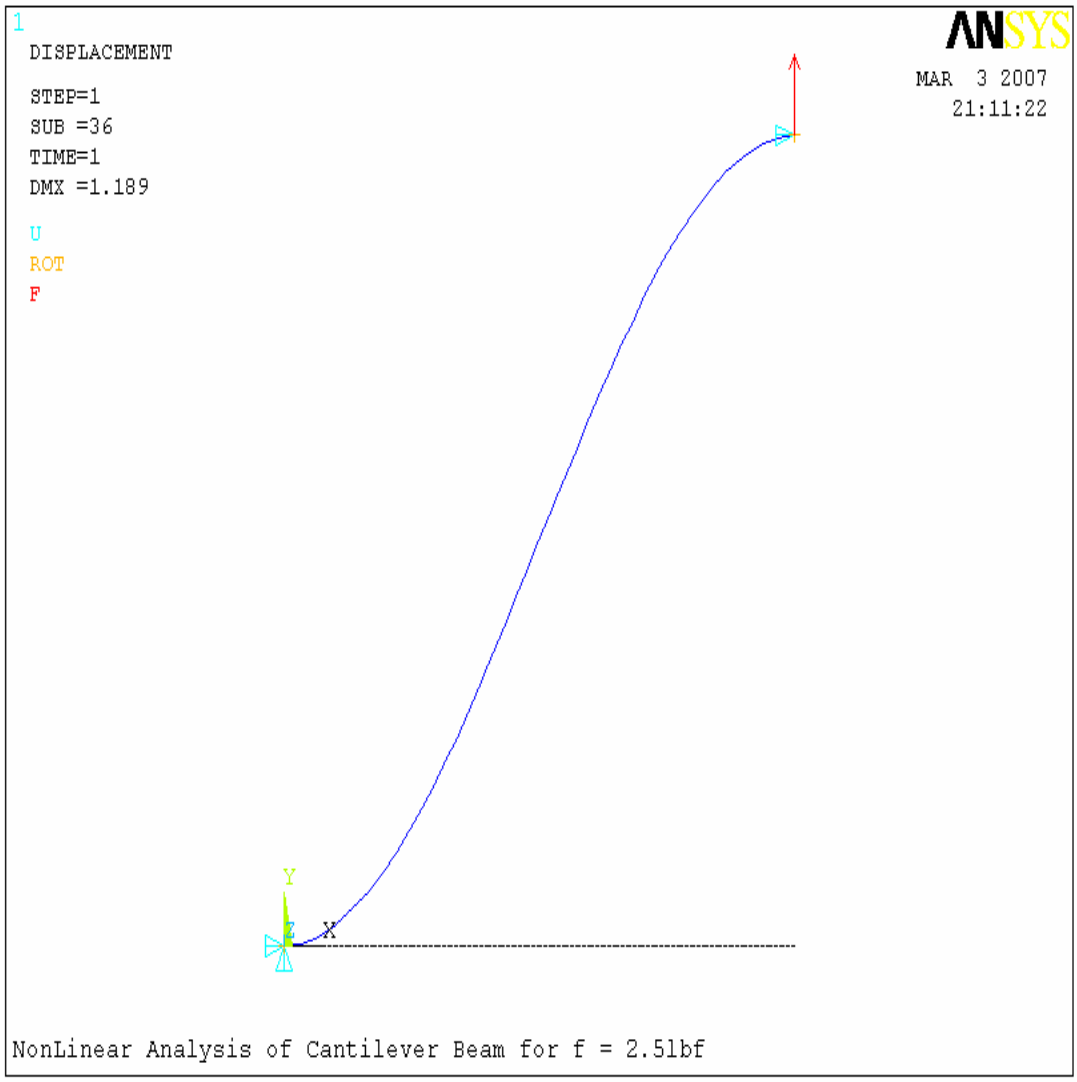

Fig 6.20 Force is equal to 2.5 lbf

6.7 Blunt Dissection

Equations from (5.1) to (5.29) in chapter 5 were used to implement the *blunt dissection* based on the parameters described in section 6.5 and the phenomenon was simulated in real time using *VC++* and *OpenGl.* We show the different steps in the *blunt dissection* from figure 6.21 to figure 6.28. Figure 6.28 shows the rupturing of the organ under the action of stress (bending plus axial) when it is more than the threshold.

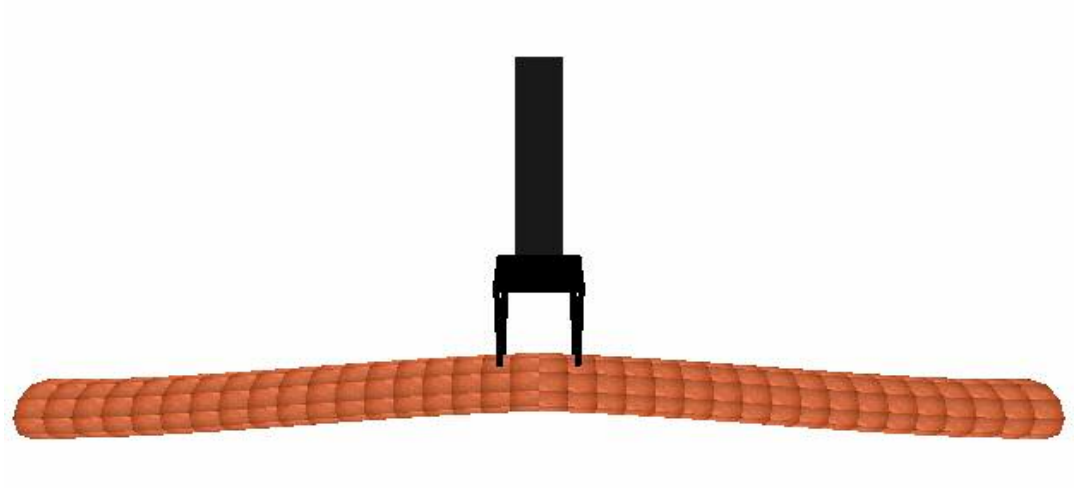

Fig 6.21 Blunt Dissection Step 1

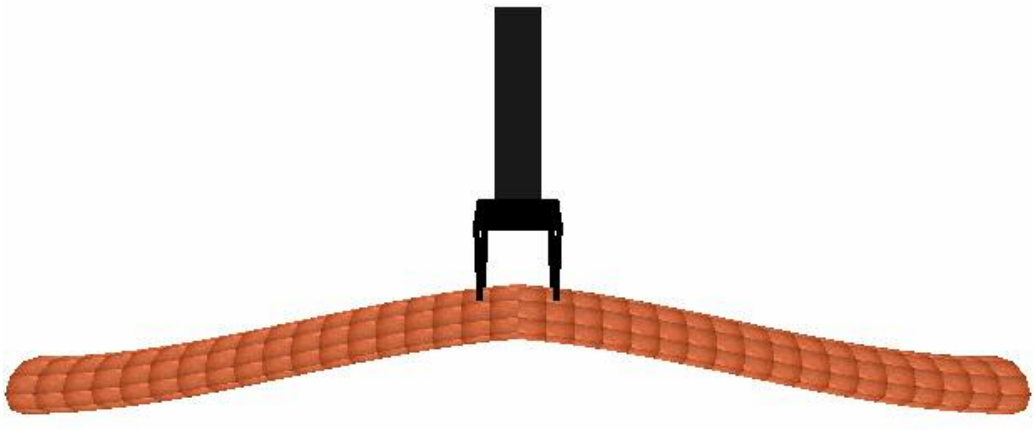

Fig 6.22 Blunt Dissection Step 2

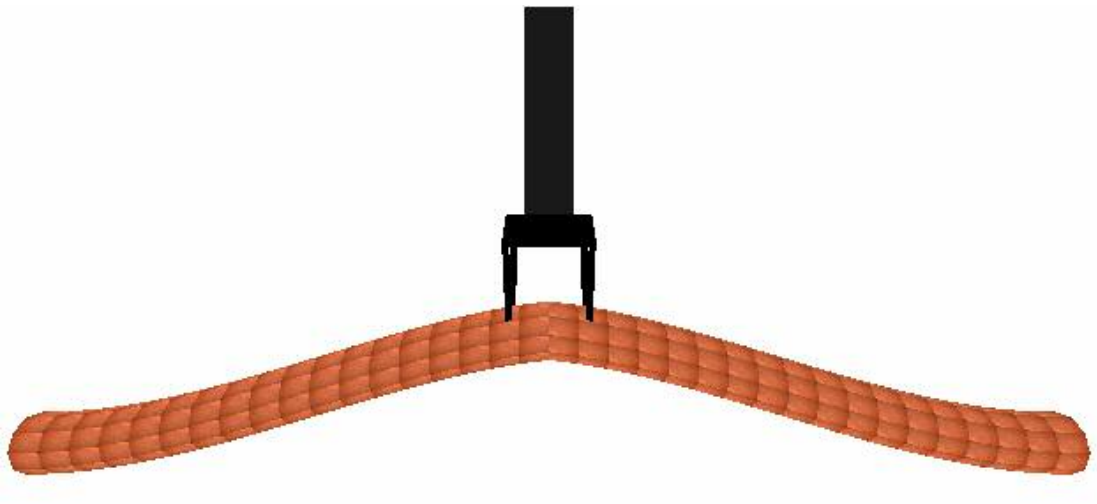

Fig 6.23 Blunt Dissection Step 3

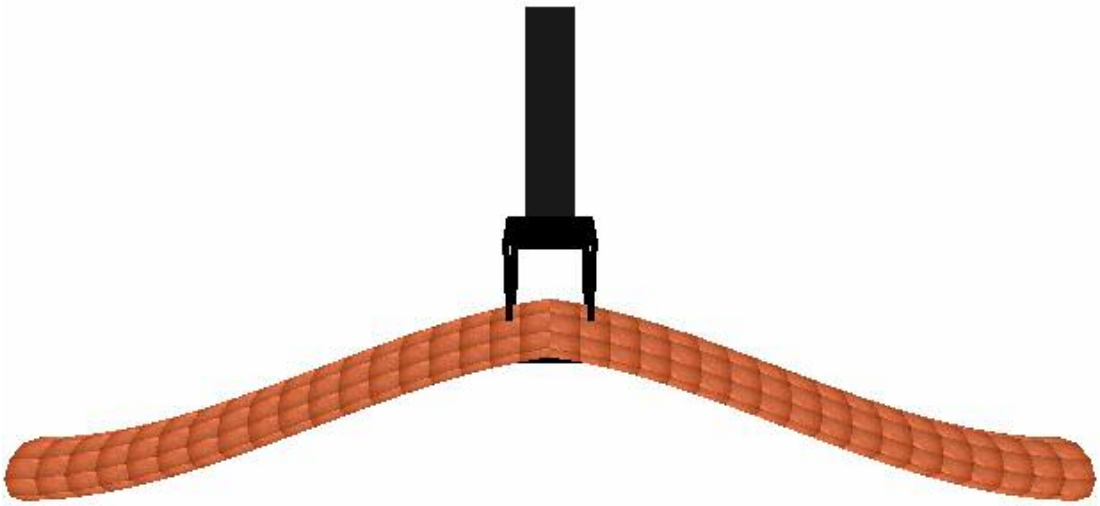

Fig 6.24 Blunt Dissection Step 4

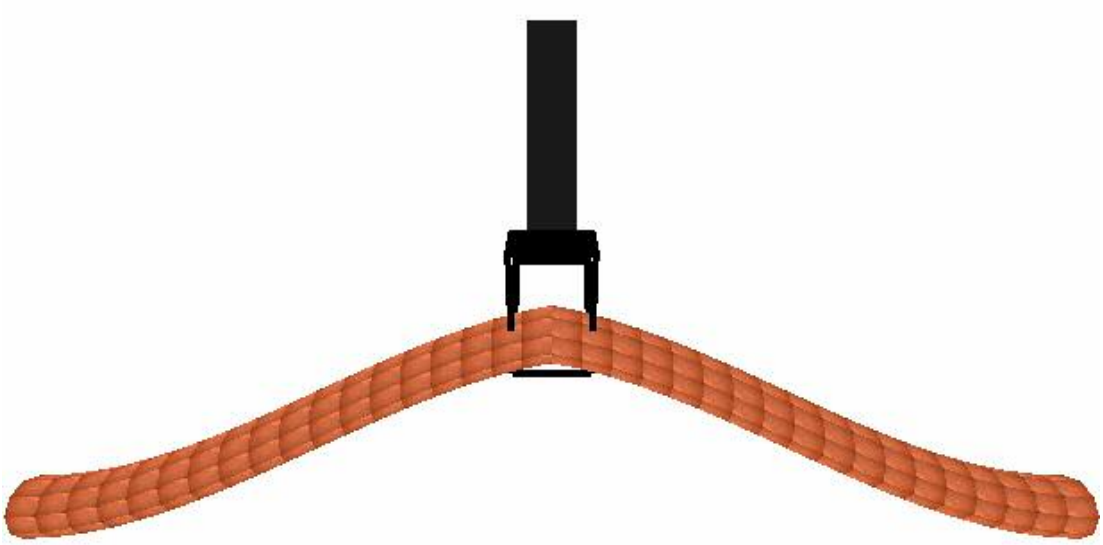

Fig 6.25 Blunt Dissection Step 5

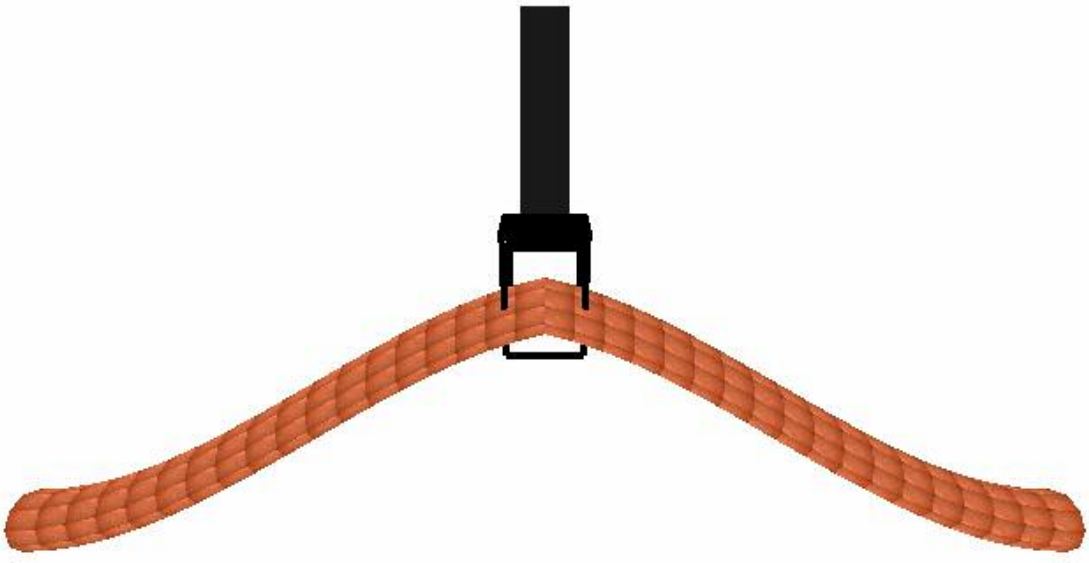

Fig 6.26 Blunt Dissection Step 6

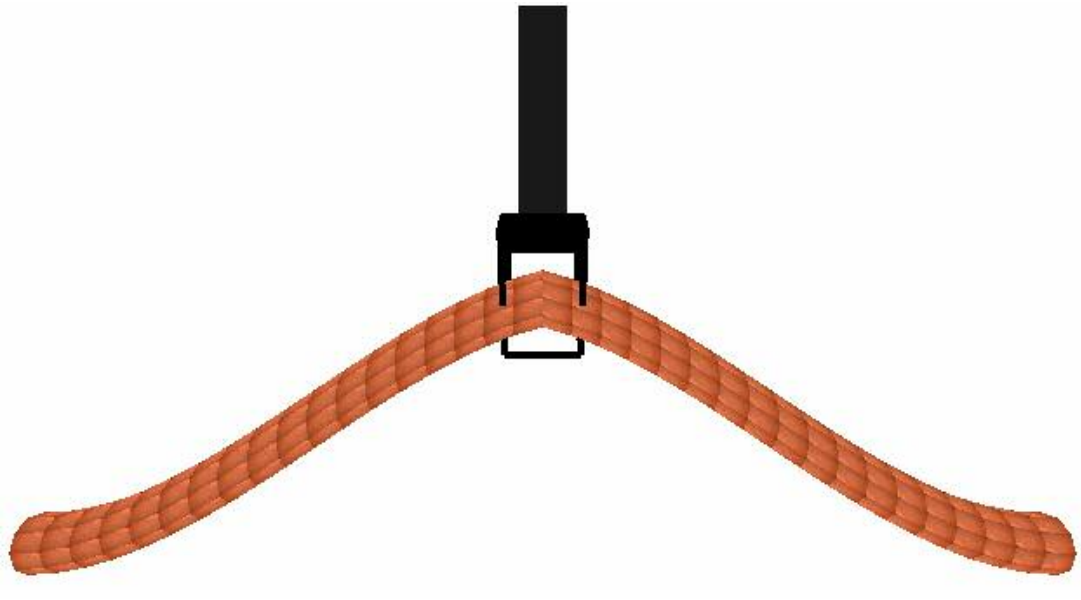

Fig 6.27 Blunt Dissection Step 7

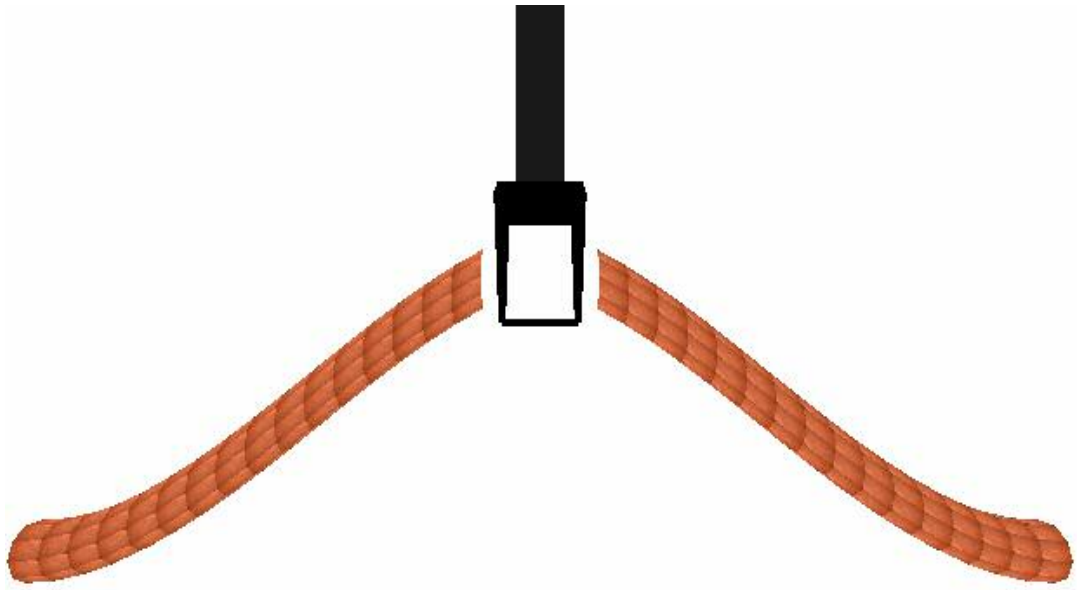

Fig 6.28 Blunt Dissection Step 8: Implementation of *blunt dissection* Step at $P = 0.4$ lbf

CHAPTER 7

MODELING OF AN ORGAN USING A BEAM MODEL

Now that we have validated the mathematical model of an organ, we investigate some practical aspects of using the model in the actual simulation of an organ. One of the key factors in simulation is to keep the computational burden under control so as to enable the real time implementation. For *bile duct*, constant circular cross sections of our beam model can be assumed. But this may not be true for other organs. Hence we have developed a new method for representing organs graphically hereafter.

Cross-sectional images have been traditionally used to create models of organs [9]. But these spline based methods are computationally expensive. In figure 7.1, on the left hand side we illustrate a long and tubular organ. Our intent now is to use the beam equations developed in the previous chapter to simulate an organ in a computer. Our graphical representation of a beam essentially consists of *key* and *driving* points (see figure 7.1). For calculating the coordinates of these points, we first take several cross-sections of the organ and find the edges of the cross-section using an edge detector algorithm. Once the edge points have been located, we fit two 6^{th} order curves of the form $y = a_o + a_1 x + a_2 x^2 + a_3 x^3 + a_4 x^4 + a_5 x^5 + a_6 x^6$, one to the top half and the other to the bottom half of the cross-section using least squares fitting. The particular cross-section can now be represented simply by two equations, instead of a large collection of points.

Now we attempt to compress the information needed to store the model using the following strategy. If the cross-section of the organ does not change over a certain length, no information needs to be stored for that length of the organ. A set of equations can effectively be used to represent a section of the organ as long as the *root mean square error* between the first set of equations and the equations after a small distance of the organ remains below a certain threshold. We can thus reduce the number of cross-sections and points to create the model.

Computational burden to simulate large deflection and hence the *blunt dissection* using the proposed approach will be much less than any other conventional method because once we calculate the deflection of the axis of symmetry all other points can be evaluated using a proper transformation matrix instead of computing a stiffness matrix [2] or per node analysis [5].

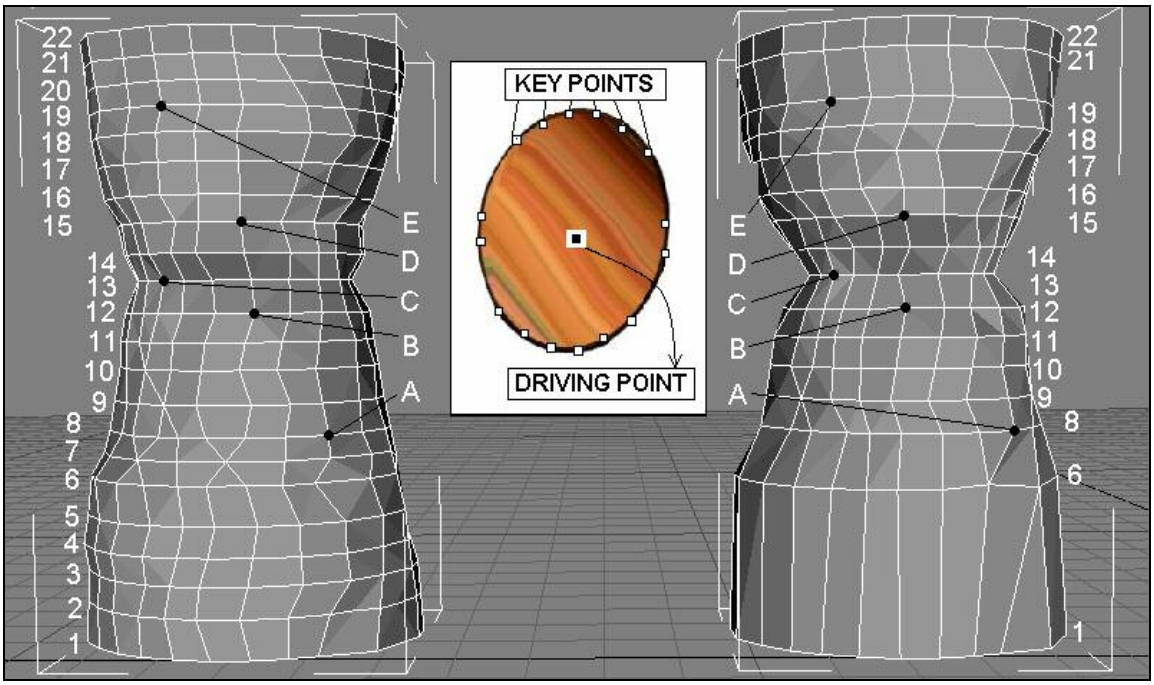

Fig 7.1 All cross sections (left), after discarding (right side), key and driving points (middle)

We conclude therefore, that given the mathematical model developed in the thesis, supported by the validation and the initial evaluation of a graphical representation of an organ using this approach, a real time simulation is entirely feasible.

CHAPTER 8

CONCLUSIONS AND SUGGESTIONS FOR FUTURE WORK

Our beam model will be the first of its kind which can simulate in large and small deflection real time with a precision. Also as the number of key and driving points reduced using our method of organ modeling, the simulation becomes faster. The numerical solution for the complex equation (5.6) works in real time with less than 4 iterations to converge. We use standard numerical methods like Newton's – Raphson method to iterate and solve.

Future work should attempt to complete a graphical and haptic simulation of a tubular organ within the large surgical framework developed at Virtual Environment Laboratory (VEL), UTA. This could be a part of the present Inguinal Herniorrhaphy. Secondly, deformation of any odd shape organ is important which may not be necessarily tubular in shape.

REFERENCES

[1] R. Frisch-Ray, *Flexible Bars*, Butterworths, London, 1962.

[2] Robert D. Cook, *Finite Element Modeling for Stress Analysis*, John Wiley, 1995.

[3] Richard G. Budynas, *Advanced Strength and Applied Stress Analysis*, 2nd Edition, Mc Graw Hill Book Co., 1999.

[4] Platt S. M. and Badler N. I., "Animating facial expressions", *in the proceedings of SIGGRAPH'81*, ACM Press, pp. 245 -252, 1981.

[5] Waters K., "A muscle model for animating three-dimensional facial expression", *ACM Computer Graphics*, vol. 21, no. 4, pp. 17-24, 1987.

[6] Terzopoulos D. and Waters K., "Physically – based facial modeling, analysis and animation", *Journal of Visual and Computer Animation*, no.1, pp. 73-80, 1990.

[7] Baraff D. and Witkin A., "Large steps in cloth simulation", *in the proceedings of SIGGRAPH*, pp. 43 -52, 1992.

[8] Baraff D. and Witkin A., "Dynamic simulation of non – penetrating flexible bodies", *in the proceedings of SIGGRAPH*, pp. 303-308, 1992.

[9] Beylot P., Gingins P., Kalra P., Magnenat Thalmann N., Maurel W., Thalmann D. and Fassel J., "3D Interactive Topological Modeling using Visible Human Dataset", *in Eurographics '96*, Blackwell Publishers, pp. C33-C44, 1996.

[10] Bro-Nielsen M., "Surgery simulation using fast finite elements", *in VBC'96: proceedings of the 4th International Conference on Visualisation in Biomedical Computing*, Springer – Verlag (London: UK), pp. 529-534, 1996.

[11] De S. and Bathe K. J., "The method of finite spheres", *Comp. Mechanics*, vol 25, pp. 329-345, 2000.

[12] Brown J., Montgomery K., Latombe J.C. and Stephanides M., "A microsurgery simulation system", *in Medical Image Computing and Computer – Assisted Interventions*, pp. 137 – 144, 2001.

[13] Giacomo T. and Magnenat-Thalmann N., "Bi-layered mass-spring model for fast deformations of flexible linear bodies", *in Conf. Rec. 2003 IEEE 16th Int. Conf. on Computer Animation and Social Agents*, pp. 48 – 53, 2003.

[14] Berkley J., Turkiyyah G., Berg D., Ganter M. and Weghorst S., "Real-Time Finite Element Modeling for Surgery Simulation: An Application to Virtual Suturing", *IEEE Transactions on Visualizations and Computer Graphics*, vol 10, pp. 314 – 325, 2004.

[15] Duch U. Birgitte, Andersen Helle and Gregersen Hans, "Mechanical properties of the porcine bile duct wall", *Biomedical Engineering Online*, vol 3, 2004.

[16] Wang X. and Devarajan V., "2D structured mass spring system parameter optimization based on axisymmetric bending for rigid cloth simulation", *in the proceedings of ACM SIGGRAPH international conference on Virtual-Reality Continuum and its applications in Industry*, pp. 317-324, 2004.

[17] Shen Y., Devarajan V. and Eberhart R., "Haptic herniorrhaphy simulation with robust and fast collision detection algorithm", *in the proceedings of Medical Meets Virtual Reality,* pp. 458-464, 2005.

[18] Wang X. and Devarajan V., "1D and 2D structured mass –spring models with preload", *Visual Computer*, vol 21, pp. 429-448, 2005.

[19] Dalmiya V., Tandon S., Mohanraj P. and Devarajan V., "Determination of key and driving points a beam model for the simulation of tissues", *in the proceedings of Medical Meets Virtual Reality 15*, pp. 106 -108, 2007.

[20] Dalmiya V., Ramirez G. and Devarajan V., "Modeling of Isotropic Organs using beam models for the Haptic simulation of blunt dissections", *in the proceedings of Medical Meets Virtual Reality 15*, pp. 100 -105, 2007.

[21] Sahai T.S., Bhiladvala R.B. and Zehnder A.T. "Thermomechanical transitions in doubly-clamped micro-oscillators", *International Journal of Non –Linear Mechanics*, in press 2007.

[22] Wang X. "Deformable Haptic models for Surgical Simulation", PhD Dissertation, The University of Texas at Arlington, 2005.

[23] Dr.Tyrone Peter Sangster. M.D; C.P.H; D.G.S, *An overview of laparoscopic dissection modalitie*, http://www.laparoscopyhospital.com/dissection.htm.

[24] SAGES Top 12 Procedures, "Every resident and practicing surgeon should know", vol 2.

BIOGRAPHICAL INFORMATION

Vishal Dalmiya earned his Bachelor of Electrical Engineering from Jadavpur University, India in 2004. He worked with Siemens Ltd. from 2004 to 2005 and was recognized for the project he developed for the company to reduce cost in terms of man power and investment. He is currently a Masters student at the University of Texas (UTA), Arlington in the Department of Electrical Engineering. He is pursuing his research in the field of surgical simulation in the Department of Electrical Engineering. He is the group leader at the Virtual Environment Laboratory in UTA. He is the recipient of Dean Master's Fellowship for his studies in the University of Texas, Arlington. He has also received the title of University Scholar for his academic and research achievements in 2007 at UTA.